https://doi.org/10.5194/egusphere-2025-3666
Preprint. Discussion started: 16 September 2025

Decoded Antarctic snow accumulation history reconciles observed and modeled trends in accumulation and large-scale warming patterns

David P. Schneider[1], Ziqi Yin[2], Gemma K. O'Connor[3], Edward Blanchard-Wrigglesworth[4], Zaria I. Cast[5], Rajashree Tri Datta[6], Zachary I. Espinosa[4]

[1]Cooperative Institute for Research in Environmental Sciences, University of Colorado Boulder, Boulder, CO 80309 USA
[2]Department of Atmospheric and Oceanic Sciences, University of Colorado Boulder, CO 80309 USA
[3]School of Oceanography, University of Washington, Seattle, WA 98195 USA
[4]Department of Atmospheric and Climate Science, University of Washington, Seattle, WA 98195 USA
[5]National Snow and Ice Data Center, University of Colorado Boulder, CO 80309, USA
[6]Department of Geoscience and Remote Sensing, TU Delft, 2628 CN Delft, The Netherlands

Correspondence to: David P. Schneider (snow.heaving335@passmail.net)

https://doi.org/10.5194/egusphere-2025-3666
Preprint. Discussion started: 16 September 2025

Abstract.

Ice-core reconstructions indicate that increased snow accumulation on the Antarctic Ice Sheet mitigated global sea level rise by ~ 11 mm during 1901-2000. However, in the most recent 40 years of more intense observation and warming, the trend in the Antarctic-wide accumulation rate has been negligible. We attribute these trends by evaluating Earth system model experiments in comparison with dynamically consistent reconstructions of surface climate. Single-forcing experiments reveal that rising concentrations of greenhouse gases (GHGs) have been the underlying driver of increased accumulation, yet acting alone would have caused twice the observed accumulation-related sea level mitigation during 1901-2000. Aerosol-driven cooling partially compensates this overprediction, but there is strong evidence for other processes at work. We hypothesize that high-latitude winds have been working together with ice-shelf meltwater fluxes to dampen Southern Ocean surface warming and suppress the GHG-driven accumulation increase since the initiation of West Antarctic ice shelf thinning in the mid-twentieth century. The wind pattern associated with strengthening of the Southern Hemisphere westerlies and deepening of the Amundsen Sea Low distributes accumulation unevenly across the continent in an orographic pattern that is consistent across models and the reconstructions. In reconstructions, these same wind and accumulation patterns are associated with muted surface warming across the eastern Pacific and Southern Ocean, a pattern not captured in climate projections including the all-forcings large ensemble studied here. However, the westerly wind history constrained by paleoclimate data assimilation largely reconciles differences between the model's ensemble-mean response and the observed world for both Antarctic-wide accumulation and large-scale warming patterns. Although the large ensemble simulates similar wind histories to the real one, its corresponding responses in SSTs and Antarctic-wide accumulation are decoupled from the wind. We discuss how this significant observation-model discrepancy, which has widespread implications for projecting regional climate change, likely arises from omitted meltwater forcing and/or resolution limitations. As a component of the sea level budget and a gauge of the magnitude and spatial pattern of climate change, Antarctic snow accumulation is a critical target for models to replicate.

https://doi.org/10.5194/egusphere-2025-3666
Preprint. Discussion started: 16 September 2025

1 Introduction

The Antarctic Ice Sheet (AIS) has been losing mass for at least the past four decades, primarily via enhanced ice discharge induced by ice-shelf basal melting, contributing to global sea level rise (e.g. Rignot et al., 2019; Velicogna et al., 2020; Fox-Kemper et al., 2021). The rate of mass loss has generally been accelerating since the 1980s (Rignot et al., 2019; Shepherd et al., 2019), but gravity anomalies from satellite data suggest that changes in snow accumulation have modulated this rate, even slowing it down during 2016-2019 (Velicogna et al., 2020). Record-high accumulation years have occurred in the early 2020s (Clem et al., 2023; Wang et al., 2025), in part associated with the anomalous heat and moisture delivered during atmospheric river events (e.g. Blanchard-Wrigglesworth et al., 2023; Wille et al., 2025). However, the consensus among multiple studies employing observation-constrained physical models is that there has been no significant trend in the Antarctic-wide accumulation rate since 1980 despite significant climate warming (e.g. Lenaerts et al., 2019; Mottram et al., 2021; Clem et al., 2023; Jones et al., 2019). The lack of an accumulation trend may be linked to the surface cooling of the Southern Ocean (e.g. Fan et al., 2014; Kang et al., 2023), increased Antarctic sea ice extent during 1979-2014 (e.g. Fan et al., 2014; Blanchard-Wrigglesworth et al., 2021) or strengthening of the circumpolar westerly winds (Medley and Thomas, 2019), but the exact cause has not been determined.

Snow accumulation is the only mass input to the AIS; its time-averaged value is ~ 2000 Gt yr^{-1} over the grounded AIS (Mottram et al., 2021; Dunmire et al., 2022), or ~ 6 mm of sea level equivalence (SLE). As such, modest changes to the accumulation rate, especially when sustained over multiple years, affect the overall mass balance of the AIS and its contribution to sea level. In the short term, an increase in accumulation represents an increase in mass storage on the AIS, thereby removing this mass from the ocean and causing a relative lowering of sea level. Although here we focus on the immediate potential sea level mitigation from increased Antarctic accumulation, over multiple decades to centuries, increased mass input may enhance the driving stress of outlet glaciers, accelerating their discharge of ice into the ocean (Winkelmann et al., 2012).

Given that AIS mass balance is the largest source of uncertainty in global sea level projections (Fox-Kemper et al., 2021), constraining the mass input from accumulation is a scientific imperative. Climate model projections suggest that annual Antarctic snowfall (the dominant term in snow accumulation) could increase by up to 43% during the twenty-first century (Palerme et al., 2016), in accordance with thermodynamics governing the increased moisture holding capacity of the atmosphere with warming. Yet, these projections differ widely, and direct comparisons between observations and Earth system models are rare, with some studies suggesting that models underpredict accumulation trends (e.g. Medley et al., 2018) and others suggesting that they overpredict them (e.g. Dunmire et al., 2022). Reconstructions that combine temporal information from ice cores with spatial relationships from models or reanalysis offer a new opportunity for model evaluation over long time periods. Medley and

https://doi.org/10.5194/egusphere-2025-3666
Preprint. Discussion started: 16 September 2025

Thomas (2019) find that increased accumulation mitigated sea level rise by ~ 10 mm during the twentieth century. Wang and Xiao (2023) report ~14 mm over the 1901-2010 period.

To date, there has been little attention given to evaluating the quantitative agreement between the reconstructions and climate models, nor to attributing the changes to specific climate forcings, such as changes in greenhouse gas concentrations, aerosols and stratospheric ozone. Such evaluations and attributions are critical for understanding the climatic factors that affect the AIS and for gaining confidence in model-based projections of accumulation and sea level. We are therefore motivated to evaluate the agreement between reconstructed snow accumulation and a current-generation climate model over the twentieth century, and to use the same model to assess the main drivers of historical change and constrain future projections. This single-model framework allows the drivers of the accumulation trend, including different external forcings, internal variability, and SST patterns, to be more explicitly identified than is possible using multi-model analyses. It also enables observations to be directly used in the model framework in unique and complimentary ways, including SST and wind nudging, as well as paleoclimate data assimilation. Besides attribution, a primary goal of this study is to bridge the gap between observed and modeled accumulation trends over the longest record possible. Antarctic precipitation variability is tightly embedded within the large-scale climate system (Genthon et al., 2004). By leveraging snow accumulation archives, this evaluation contributes to understanding systematic discrepancies between observed and modeled trends within the climate system (e.g. Wills et al., 2022; Simpson et al., 2025).

2 Data and Methods

2.1 Model description and primary metrics

Most experiments discussed here (Table 1) employ the Community Earth System Model, version 2 (CESM2), a comprehensive model with coupled land, atmosphere, sea ice and ocean components (Danabasoglu et al., 2020). CESM2 represents Antarctica surface climate and the processes that affect snow accumulation very well, improving upon its predecessor, CESM1 (Dunmire et al., 2022). Here, we use the term “snow accumulation” or simply "accumulation" for consistency with Medley and Thomas (2019) and to emphasize that accumulation is the only mass input to the AIS. “Surface mass balance (SMB)” has the same meaning as our formulation of accumulation. CESM2 does not have an interactive Antarctic Ice Sheet or ice shelves.

Dunmire et al. (2022) report that CESM2 simulates an unrealistically large, upward trend in Antarctic accumulation for the 1979-2015 period, which they attribute to CESM2's equilibrium climate sensitivity (ECS) of ~5 K (Gettleman, Hannay et al., 2019), which is greater than observationally constrained estimates of ECS suggest (Armour et al., 2024). However, when observed SST warming patterns are

https://doi.org/10.5194/egusphere-2025-3666
Preprint. Discussion started: 16 September 2025

accounted for, high-ECS models have a lower *effective* climate sensitivity (Armour et al., 2024). This is explained by the SST pattern effect, which describes the dependence of radiative feedbacks on the spatial pattern of surface warming (Andrews et al., 2022). In observations, the Southern Ocean and eastern Pacific have cooled in recent decades, in contrast to the warming simulated by CESM2 and many other CMIP6 models (Wills et. al, 2022). In CESM1 (Hurrell et al., 2013) at least, introducing Antarctic observational data into the model via enhanced meltwater fluxes or wind nudging brings simulated SST and sea level pressure trends into better agreement with observations (Dong et al., 2022a; Armour et al., 2024). However, it has yet to be demonstrated that reduced Southern Ocean warming lowers the Antarctic accumulation rate. To test this idea, we exploit the many realizations of internal variability within a large ensemble and examine accumulation trends in several experiments constrained by observations.

We compare snow accumulation simulated by CESM2 with the gridded reconstruction of Medley and Thomas (2019) (hereafter, 'MT19' or 'reconstruction'), favoring this reconstruction because it is accessible, well verified and has been used in previous work with CESM2 (Dunmire et al., 2022). It was calibrated to the spatial signature of precipitation minus evaporation (*P minus E*) in the MERRA2 atmospheric reanalysis (Gelaro et al., 2017), with a bias correction based on accepted *in-situ* measurements. We specifically use the version remapped by Dunmire et al. (2022) from its native resolution to the standard grid of CESM2's land and atmosphere components. It spans 1801-2000 at annual resolution.

Our primary metric of snow accumulation is the timeseries of cumulative mass change over the grounded AIS relative to a pre-industrial baseline (Appendix A). This metric de-emphasizes the large temporal variability of precipitation (Previdi and Polvani, 2016) making for a less noisy data-model comparison, and permits the time-integrated signals of climate forcings (Casado et al., 2023) to be detected. The spatial patterns of snow accumulation trends are also indicators of the responsible climate drivers; pattern correlations (Appendix A) between reconstructed and modeled trends are adopted as secondary metrics for interpreting the Antarctic snow accumulation history. Signatures of atmospheric circulation variability are prominent in Antarctic accumulation records (e.g. Medley and Thomas, 2019; Genthon et al., 2004), making it imperative to account for these impacts to uncover the underlying warming-driven trends. As such, we calculate a wind index that captures the dominant circulation variability and determine the trends in accumulation that are congruent with trends in this index (Appendix A). In turn, this index ties Antarctic accumulation to the broader-scale climate system.

2.2 CESM2 Experiments

Our evaluation leverages a suite of previously published CESM2 experiments (Table 1). The first four ensembles comprise the single-forcing large ensemble (Simpson et al., 2023), whose forcings added together are the same external forcings as in the half of the 100-member CESM2 Large Ensemble (CESM2-LE) that has smoothed biomass burning (Rodgers et al., 2021). The other half of the Large Ensemble, denoted as CESM2-LEcmip6, uses the standard CMIP6 historical forcing with a few

https://doi.org/10.5194/egusphere-2025-3666
Preprint. Discussion started: 16 September 2025

exceptions (Rodgers et al., 2021; Danabasoglu et al., 2020). Hereafter the text will use "Large Ensemble" to generally refer to the whole ensemble. The tropical Pacific pacemaker experiment, TPACE, constrains the evolution of internal variability in the model by nudging it towards observed SST anomalies in tropical Pacific. SSTs outside of the nudged region are free to evolve. Given the ubiquitous role of tropical teleconnections in Antarctic climate variability (e.g. Li et al., 2021; Schneider et al., 2012), the pacemaker setup is an important way to constrain simulations with observations. In addition to the synching of internal variability, it can also help account for biases in the model's forced response. Stratospheric ozone depletion and recovery is represented in the Large Ensemble, TPACE and "everything else" (EE) ensembles, but its role cannot be isolated with these experiments, as was done in experiments with CESM1 (Lenaerts et al., 2018; Chemke et al., 2020; Schneider et al., 2020).

We use the data-rich period since 1979 to evaluate multiple observation-constrained simulations (Table A1) and their depictions of the spatial patterns of snow accumulation change. These experiments include a coupled wind nudging experiment, uncoupled prescribed SST and sea ice experiments, and a coupled meltwater experiment to explore specific mechanisms of accumulation change, and directly link Antarctic accumulation with the observed SST and sea ice record. Appendix A has further details.

The ensemble mean of a large ensemble smooths out the signals of internal variability arising from the initial conditions, revealing the model's response to the external radiative forcings (greenhouse gasses, aerosols, etc.) imposed in the experiment. In this text, the forced response is denoted by square brackets, for example "[GHG]" for the ensemble-mean of the greenhouse gas single forcing ensemble. The internal component of a given ensemble member is found by removing the forced response from that member. Similarly, to isolate the role of the tropical SST nudging in the TPACE experiment, [CESM2-LE*] is subtracted from [TPACE], where [CESM2-LE*] is the ensemble-mean of the 10 members of CESM2-LEcmip6 that have the same piControl initialization states as the 10 members of TPACE.

https://doi.org/10.5194/egusphere-2025-3666
Preprint. Discussion started: 16 September 2025

190

Table 1. Summary of coupled CESM2 experiments used for cumulative mass gain calculations and spatial trend illustrations. All experiments use the standard 1° x 1° horizontal resolution and all (except piControl) follow the SSP3-7.0 forcing scenario from 2015 onwards. Figure 2 and Table 2 show uncertainty estimates of the cumulative mass gain.

abbreviation	years integrated	evolving radiative forcing	SSTs, sea ice	purpose	ensemble members	ens. mean mass gain 1901-2000
GHG	1850-2050	anthropogenic greenhouse gases	coupled	evaluate forced response to greenhouse gases	15	7483 Gt
AAER	1850-2050	anthropogenic industrial aerosols (CMIP6)	coupled	evaluate forced response to anthropogenic industrial aerosols	20 (15 for GHG + AAER)	-3156 Gt (GHG + AAER = 4185 Gt)
BMB	1850-2050	biomass burning aerosols (smoothed)	coupled	evaluate forced response to biomass burning aerosols	15	-281 Gt
EE	1850-2050	stratospheric & tropospheric ozone; solar variability; volcanic aerosols; EE = 'Everything Else'	coupled	evaluate forced response to natural and anthropogenic forcings not included in GHG, AAER or BMB	15	745 Gt
CESM2-LE	1850-2100	all major natural and anthropogenic forcings from CMIP6 (with few exceptions, Danabasoglu et al. (2020)), with smoothed biomass burning	coupled	evaluate response to combined forcings; separate forced response from internal variability	50	6079 Gt
CESM2-LEcmip6	1850-2100	all major natural and anthropogenic forcings, including original CMIP6 biomass burning aerosols	coupled	as above; also used as prior for PDA	50	6434 Gt
TPACE	1880-2019	as in CESM2-LEcmip6	coupled; nudged to SST anomalies (ERSSTv5) in trop. Pacific	sync the model to evolution of observed variability in the tropical Pacific in the context of evolving radiative forcing	10	4167 Gt
CESM2-LE*	1850-2100	as in CESM2-LEcmip6; members with same initial conditions as TPACE	coupled	baseline to isolate impacts of SST nudging in TPACE	10	6478 Gt
piControl	1000 years	pre-Industrial control; forcings fixed at nominal 1850 values	coupled	evaluate climate system behavior in the absence of anthropogenic forcing; calculate baseline Antarctic snow accumulation rate	1	mean of 24 century-length segments: -186 ±1114 Gt

195

2.3 Reconstructions using paleoclimate data assimilation

To help illustrate and quantify the role of atmospheric circulation and surface temperatures over the entire twentieth century, we employ annually resolved reconstructions of near-surface zonal winds, sea

https://doi.org/10.5194/egusphere-2025-3666
Preprint. Discussion started: 16 September 2025

level pressure (SLP) and surface air temperature (SAT) generated by paleoclimate data assimilation (PDA). We first use the reconstruction presented in O'Connor et al. (2021) that uses members of the CESM1 Large Ensemble (Kay et al., 2015) to form the prior. The global proxy network includes Antarctic ice core data used in the MT19 reconstruction. This reconstruction, while skillful in the regions of interest to this study, is not fully dynamically consistent with the CESM2 experiments evaluated here. We therefore utilize a new PDA reconstruction following the same methodology and using the same global proxy network, but with the prior formed by the first seven members of CESM2-LEcmip6 (O'Connor et al., in press). Use of both CESM1-LE PDA and CESM2-LE PDA has some advantages. While both reconstructions skillfully estimate the Amundsen Sea Low (ASL) Index (Fig. 1a) and other aspects of the dynamics represented by winds and sea level pressure (Fig. B1), there are marked differences in their surface temperature reconstructions (Figs. B2, B3). Based on considerations discussed in Appendix B, we regard the CESM1-LE PDA as the more reliable of the two surface temperature reconstructions.

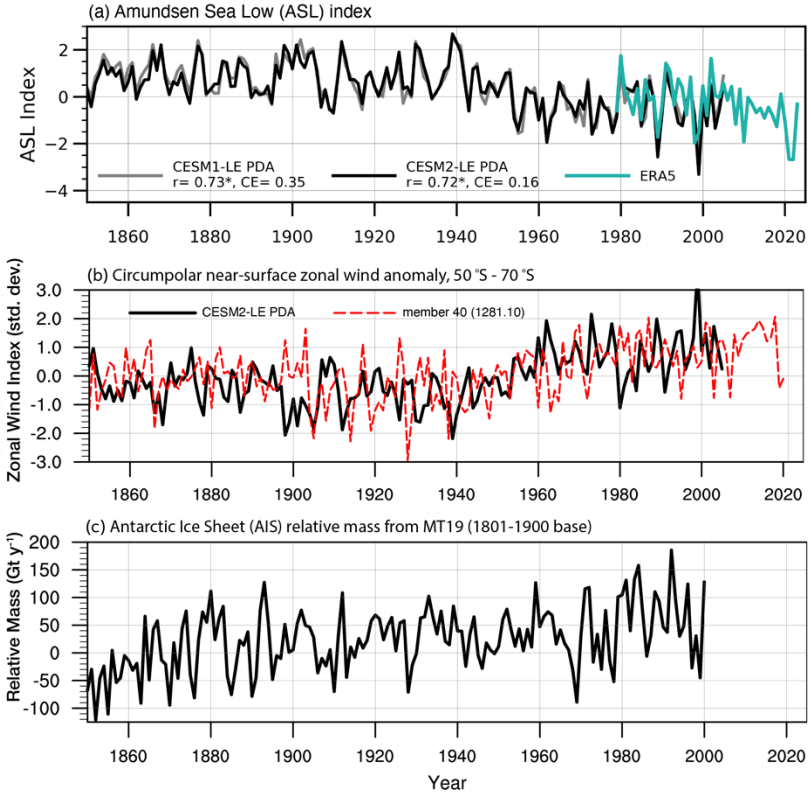

Figure 1. a) Timeseries of annual-mean Amundsen Sea Low (ASL) index from two different instances of PDA, compared with ERA5. Anomalies relative to 1979-2005. The ASL Index is the standardized mean SLP over 60º-75º S, 180º-310º E; b) Standardized, annual mean, near-surface zonal wind indices across 50º S-70º S from CESM2-LE PDA and member 40 of CESM2-LEcmip6 (using 10 m zonal wind). The 1901-2000 trend in the CESM2-LE PDA zonal wind index is statistically significant ($p < 0.01$); c) Relative mass timeseries integrated over the grounded AIS from MT19 snow accumulation reconstruction. Base period is 1801-1900. The 1901-2000 trend in relative mass is statistically significant ($p < 0.05$). Over 1901-2000, detrended relative mass and the detrended zonal wind index from CESM2-LE PDA are significantly correlated ($r = -0.39$, $p < 0.01$).

https://doi.org/10.5194/egusphere-2025-3666
Preprint. Discussion started: 16 September 2025

3 Results

3.1 Cumulative AIS mass change due to snow accumulation during 1901-2000

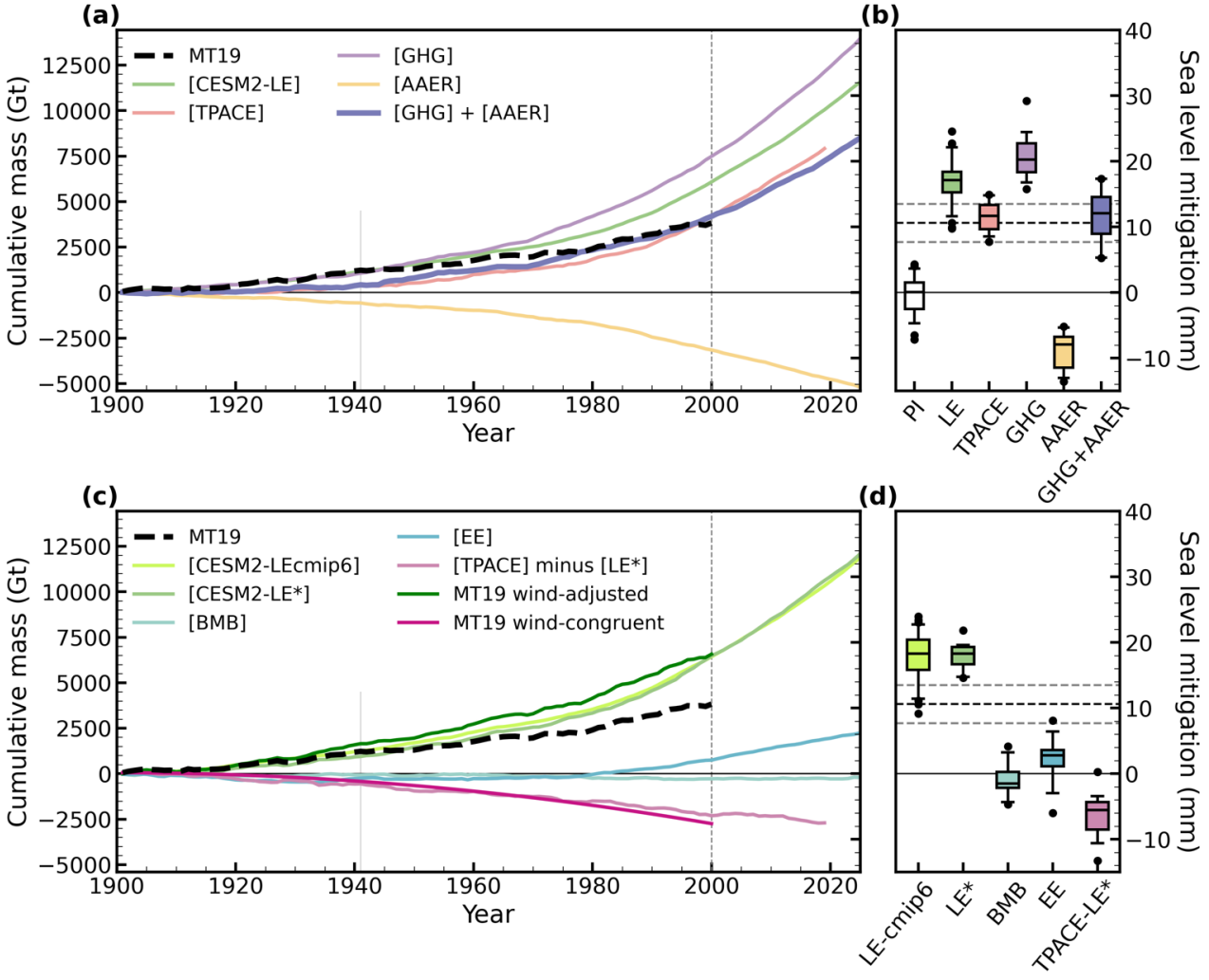

Figure 2. Cumulative mass and equivalent sea level mitigation due to accumulated snow on the grounded Antarctic Ice Sheet (AIS) in MT19 and CESM2: (a) Cumulative mass timeseries from MT19 compared with timeseries from selected ensemble means; (b) Box plot indicating ensemble spread of cumulative mass at the year 2000 for each of the ensembles and the pseudo ensemble generated by summing 15 individual members of GHG and AAER. The boxes indicate the interquartile range; the median is shown by a horizontal line. Whiskers represent the 5% and 95% bounds of the ensemble, with the values lying outside of these bounds indicated by closed black circles. "PI" refers to the piControl simulation: mass was accumulated over 24 overlapping, 100-year segments. Dashed black horizontal line indicates the mean value of MT19; gray dashed lines indicate its ± 1 σ uncertainty

https://doi.org/10.5194/egusphere-2025-3666
Preprint. Discussion started: 16 September 2025

bounds; (c) As in a), but for different ensembles and [TPACE] - [CESM2-LE*] to isolate the effect of nudging to observed tropical Pacific SST anomalies; (d) As in b), but for the ensembles shown in c).

From the MT19 reconstruction, we find a cumulative mass gain over the grounded AIS of 3824 Gt, or 10.5 mm SLE, over the twentieth century (Fig. 2a), in agreement with the 10.6 mm previously reported (Medley and Thomas, 2019). The cumulative mass gain arises because the relative mass (the annual anomaly relative to the nineteenth century; Appendix B) increases in a stepwise fashion during the twentieth century (Fig. 1c). For 1901-1925, the relative mass is about 20 Gt yr^{-1}; for 1976-2000 it is above 60 Gt yr^{-1}. The cumulative mass timeseries is highly correlated with global-mean temperature anomalies in the CESM1-LE PDA (r = 0.92; Fig. 3a). Since some common proxy data were used in MT19 and the PDA, we verify this relationship with the independent SAT dataset from ERA-20C (Poli et al., 2016), which similarly shows a high correlation with cumulative mass. Cumulative mass and global temperature anomalies are also highly correlated in CESM2 (r = 0.83 for [TPACE]). On the continental scale, both the reconstructions and the model experiments indicate a significant positive correlation between AIS-wide surface temperature anomalies and relative mass timeseries (Fig. 3b), consistent with previous work on the sensitivity of snow accumulation to temperature (Monaghan et al., 2008; Frieler et al., 2016; Dalaiden et al., 2020). Broadly, these results affirm the expectation from thermodynamics of more snow accumulation with warming (e.g. Frieler et al., 2016). However, the exact sensitivity depends on the choice of averaging period, specific experiment, and/or whether an ensemble mean or individual ensemble member is used. Global- or Antarctic- mean temperatures provide only a weak constraint on the magnitude of the snow accumulation increase and are not diagnostic of the forcings that are driving it. To understand the role of these forcings, we evaluate the suite of ensembles listed in Table 1.

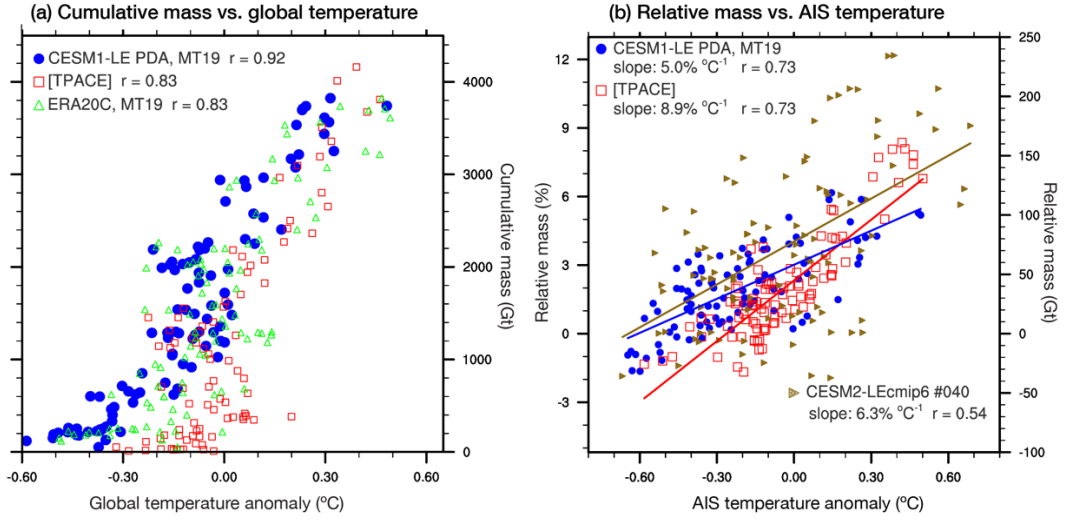

Figure 3. (a) Scatter plot of annual-mean, global-mean surface temperature anomalies versus cumulative mass timeseries over 1901-2000 with no smoothing applied; (b) Scatter plot of AIS relative mass versus AIS surface temperature anomaly, estimating the Antarctic-wide sensitivity of accumulation to temperature for selected reconstructions and CESM2 experiments. A 5 yr running mean was applied to the annual-mean timeseries before computing the regression coefficients and correlation values.

https://doi.org/10.5194/egusphere-2025-3666
Preprint. Discussion started: 16 September 2025

As shown in Figure 2, [CESM2-LE] has a mass gain of 6079 Gt (16.8 mm sea-level equivalent (SLE)), well above the MT19 reconstruction. This value is slightly higher (< 1mm SLE) in the other half of the Large Ensemble, [CESM2-LEcmip6] (Figs. 2c, 2d). While small, this difference is physically consistent with CMIP6 biomass burning forcing causing spurious warming (Fasullo et al., 2022) and supports the use of cumulative mass to track warming. Ensemble spread is indicated in the box-whisker plots (Figs. 2b, 2d). The 5% lower bound of the CESM2-LE lies within the +1 $\boldsymbol{\sigma}$ error of MT19, while two outlier ensemble members are within MT19's -1 $\boldsymbol{\sigma}$ error. Interpreting the CESM2-LE, the reconstructed cumulative mass gain of 3824 Gt could be explained by an externally forced response of 6079 Gt (16.8 mm SLE) counteracted by an internally driven mass loss of around - 2300 Gt (- 6.4 mm SLE).

Mass accumulated over century-length segments of piControl suggests that internal variability alone cannot account for the observed mass gain (Fig. 2b). Yet, as the ensemble spreads show, internal variability can partially counteract the forced response in [CESM2-LE] or [CESM2-LEcmip6] and bring model results in agreement with MT19. In the constrained TPACE experiment, mass gain is only 4167 Gt (11.5 mm SLE), just 1 mm greater than MT19 and within its 1 $\boldsymbol{\sigma}$ error (Fig. 2b). The observed trends and variability captured in TPACE reduced twentieth-century cumulative mass by 2312 Gt (6.4 mm SLE), roughly matching the magnitude of internally driven mass loss in the Large Ensemble that is required to fit the observations.

The single-forcing ensembles uncover the two major components of the forced response (Figs. 2b, 2d). Greenhouse gases are the dominant driver of the cumulative mass gain, with [GHG] giving a value of 7483 Gt (21 mm SLE), which is twice the value from the reconstruction. Aerosols offset this; mass change in [AAER] is -9 mm SLE. The sum of [GHG] and [AAER], 12 mm SLE, is within the +1 $\boldsymbol{\sigma}$ error of MT19 (Fig. 1b). The other forced responses are smaller, at 745 Gt for [EE] and -281 Gt for [BMB]. The sum of the four separate ensemble means (4698 Gt; 13 mm SLE) is near the top of the +1 $\boldsymbol{\sigma}$ error range of MT19 and in line with the ~ 14 mm SLE from the reconstruction of Wang and Xiao (2023). The result that [CESM2-LE] is ~ 4 mm SLE larger than the sum of the single-forcing ensemble means could be due to aerosol forcing alone causing a large increase in Antarctic sea ice area, but not when it acts in concert with greenhouse gas forcing (Simpson et al., 2023).

The results thus far, while showing general consistency between the CESM2 and the MT19 reconstruction, suggest two interpretations for the cumulative mass gain in MT19. Namely, the single-forcing ensembles suggest that the 10.5 mm SLE from MT19 is only due to external forcing, dominated by opposing responses to GHGs and aerosols. In contrast, the Large Ensemble and TPACE suggest a smaller role for aerosols, but a large role for internal variability in counteracting the mass gain due to GHGs. We therefore turn to the spatial patterns of snow accumulation and atmospheric circulation change to help inform the most likely interpretation of the trends. This analysis will lead to a third possibility: A portion of the mass loss that is internally driven according to the Large Ensemble and TPACE may indicate a missing and/or misrepresented external forcing.

https://doi.org/10.5194/egusphere-2025-3666
Preprint. Discussion started: 16 September 2025

3.2 Spatial patterns of snow accumulation trends and their relationships with atmospheric circulation and surface temperatures

For spatial analysis, we survey the pattern correlations between the twentieth-century trend in MT19 accumulation and each ensemble member of the Large Ensemble and TPACE, along with the ensemble means of all historical experiments from Table 1 (Figs. C1, C3). Similarly, pattern correlations for the sea level pressure (SLP) trend across 40º S - 90º S are computed with the same model experiments and using the CESM2-LE PDA as the benchmark (Figs. C2, C4). We select the ensemble member whose trend patterns in snow accumulation and atmospheric circulation exhibit the best pattern correlations to the MT19 and CESM2-LE PDA reconstructions, respectively. The best-matching individual ensemble member considering both accumulation and SLP comes from CESM2-LEcmip6.

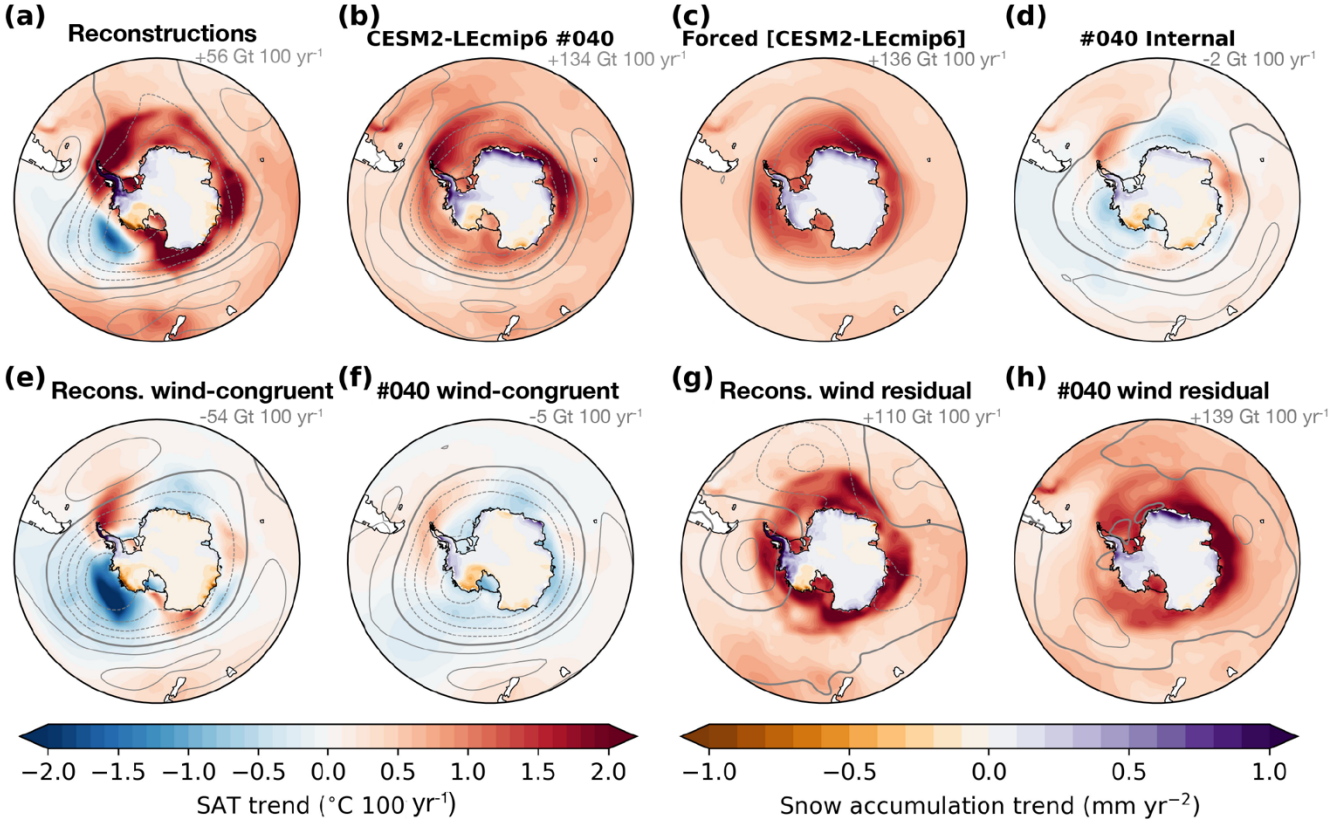

Figure 4. Linear trend patterns for 1901-2000 in annual-mean Antarctic snow accumulation rate (mm water equivalent per year), sea level pressure, and surface air temperature over the ocean from reconstructions and multiple model-based estimates. The change in the Antarctic-wide accumulation rate over the century (Gt 100 yr^{-1}) is given in the upper right of each plot: a) PDA and MT19 reconstructions; b) Ensemble member 40 of the CESM2-LEcmip6 ensemble, which has the best overall fit to reconstructed trends in SLP and snow accumulation; c) The forced component of member 40; d) The internal component of member 40; e) Trends in the reconstructions linearly congruent with the CESM2-LE PDA zonal wind index; f) Trends in member 40 linearly congruent with its zonal wind index; g) Residual trends in the reconstructions after removal of wind-congruent trends; h) Residual trends in member 40 after removal of wind-congruent trends. SLP contours (gray lines) are in intervals of 1 hPa 100 yr^{-1}. Negative SLP values are dotted lines and positive values are solid lines; the zero contour is a heavier solid line. For the PDA reconstructions, CESM1-LE PDA is used for SAT and CESM2-LE PDA is used for SLP and the zonal wind index.

https://doi.org/10.5194/egusphere-2025-3666
Preprint. Discussion started: 16 September 2025

Like the reconstructed patterns (Fig. 4a), member 40 (Fig. 4b) exhibits an accumulation trend dipole across the West Antarctic Ice Sheet (WAIS), consistent with the deepened ASL and stronger onshore onto the eastern WAIS and offshore flow from the western WAIS. On a larger scale, both member 40 and the reconstruction feature a pressure dipole between the middle and high southern latitudes, consistent with the strengthening and poleward shift of the westerlies (O'Connor et al., 2021; Dalaiden et al., 2022). Using the Large Ensemble, member 40 is separated into its forced (Fig. 4c) and internal (Fig. 4d) components. The increased accumulation rate is entirely explained by external forcing, with only a minor offset from internal variability. Using the single-forcing ensembles, the forced response patterns to individual forcings are also evaluated (Figs. C3, C4). [GHG] and [EE] are best correlated with the reconstructed SLP and accumulation patterns, but not better than the combined forced response in [CESM2-LEcmip6].

The accumulation pattern in member 40, including the dipole across the WAIS, is shaped by internal variability (Fig. 4d). In the forced response, snow accumulation increases nearly everywhere on the continent but is especially enhanced on the coasts of the WAIS and Queen Maud Land (Fig. 4c). The forced atmospheric circulation pattern indicates a strengthening and poleward shift of the westerlies, especially in the Indian Ocean sector and Drake Passage. The internally driven circulation pattern is also consistent with a strengthening of the westerlies, displaying the characteristic pressure dipole between the middle and high southern latitudes. Neither of the two circulation patterns are perfectly zonally symmetric. The forced pattern features lobes of low pressure jutting out into the eastern Ross Sea and into the south Atlantic, whereas the internal pattern features a deepened ASL, marked by low pressure anomalies in the southeastern Pacific. As discussed below, these zonally asymmetric pressure patterns are associated with zonally asymmetric SST trends in lower latitudes.

How have the strengthening westerly winds, associated with the positive phase of the Southern Annular Mode (SAM), affected accumulation? Medley and Thomas (2019) use the SAM index derived from sea level pressure data to show a reduction in accumulation related to the positive phase of the SAM for 1957-2000. Here, we use the zonal winds directly and for the full century, as provided by CESM2-LE PDA and member 40 (Fig. 1b). In the MT19 reconstruction, there is a large reduction in the Antarctic-wide accumulation rate that is linearly congruent with the significant trend in the zonal wind index (Fig. 4e). Spatially, the accumulation rate is reduced nearly everywhere on the continent expect for the Peninsula. This pattern is more weakly expressed in member 40 and there is only a small reduction in the Antarctic-wide accumulation rate associated with the winds (Fig. 4f). With wind-congruent trends removed from the reconstructions, the residual pattern exhibits a large increase in the accumulation rate associated with increased accumulation over East Antarctica, accompanied by a weaker ASL (Fig. 4g).This wind correction brings the reconstructed Antarctic-wide accumulation trend closer to the forced response given by [CESM2-LEcmip6].

The effect of tropical SST nudging in TPACE is to weaken the ASL and reduce the magnitude of the westerly wind trend (Figs. C2, C5a), resulting in a worse fit of modeled and reconstructed trend patterns than in [CESM2-LE*] (Figs. C1, C2). Nudging also drives a reduction in the Antarctic-wide

https://doi.org/10.5194/egusphere-2025-3666
Preprint. Discussion started: 16 September 2025

accumulation rate, bringing the cumulative mass gain in [TPACE] closer to the reconstruction than in [CESM2-LE*]. This suggests that it is not the winds or deepened ASL *per se* which reduce the accumulation rate. A key differentiator of the reconstructed (Fig. 4a) and modeled trend patterns (Fig. 4b) is their surface temperature trends. According to regression, reconstructed and modeled accumulation have similar sensitivities to temperature of 5-6% $°C^{-1}$ on an Antarctic-wide basis (Fig. 3b), consistent with CMIP6 multi-model consensus (Nicola et al., 2023). In the reconstruction, there is a surface cooling trend in the Pacific Sector of the Southern Ocean, especially in the Amundsen Sea near the center of the ASL. The cooling region covers the major moisture source region for snowfall on the WAIS (Sodemann and Stohl, 2009). In member 40, the Pacific Sector warms less than other regions of the Southern Ocean, but only slightly less. The wind patterns are also associated with surface cooling in the mid-latitude Indian Ocean, the major moisture source region for East Antarctic precipitation (Sodemann and Stohl, 2009). [TPACE] is also associated with muted Southern Ocean warming, but it is maximized in the Atlantic and Indian Ocean sectors rather than the Pacific (Fig. 5o).

To provide context for the polar wind and surface temperature trends, we zoom out to the entire globe (Fig. 5). The observed SST pattern from the independent ERSSTv5 dataset (Fig. 5a) is not obviously La Niña - like or El Niño - like, but it does feature less warming in the central-eastern Pacific than in the western Pacific, consistent with the strengthening Walker circulation during this time period (Lee et al., 2022) that is reflected in the zonal gradient in the SLP trend simulated by [CESM2-GOGA]. The zonal wind index from CESM2-LE PDA is congruent with cooling in the central-Eastern Pacific (Fig. 5b), in an overall pattern that closely resembles "Pattern 1" associated with observed-modeled SST trend discrepancies since 1979 (Wills et al., 2022, their Fig. 3). The wind-residual pattern is associated with enhanced eastern equatorial Pacific warming (Fig. 5c). The PDA reconstructions capture these large-scale patterns, showing muted warming in the central-eastern Pacific and enhanced warming in the western Pacific (Fig. 5d). This zonal temperature contrast is enhanced by the winds (Fig. 5e). Like in ERSSTv5, if the wind-congruent trends are removed from the reconstruction, the residual pattern shows an El Niño - like equatorial warming pattern with a weakened ASL (Fig. 5f).

The observed and reconstructed patterns can be compared to the forced responses to all forcings (Fig. 5g), aerosols only (Fig. 5h), and GHGs only (Fig. 5i) ([EE] exhibits a similar pattern to [GHG] but of much weaker magnitude, not shown). [GHG], with its El Niño - like warming pattern and north Atlantic cooling, is a good fit to the wind-residual patterns in the observations and reconstructions. Cooling in [AAER] is concentrated in the north Pacific and eastern equatorial Pacific, in disagreement with the cooling patterns associated with winds. Aggressive aerosol-driven cooling is evident in the all-forcings forced response, [CESM2-LEcmip6], which has too weak of a warming trend compared to observations and reconstructions. The Pacific zonal SST gradient in is improved in member 40 (Fig. 5j), along with the representation of the deepened ASL. However, in member 40, the winds are only associated with weak SST anomalies (Fig. 5k), and the wind-residual pattern is not El Niño like (Fig. 5l), possibly because the aerosol response in the tropics overwhelms the GHG response (Heede and Federov, 2021). The stronger zonal SST contrast and deeper ASL in member 40 are driven by a pattern of internal variability that resembles the negative phase of the Interdecadal Pacific Oscillation (IPO; Fig. 5n) defined by Henley et al. (2015). The response to nudging in TPACE (Fig. 5o) is a near mirror image to

https://doi.org/10.5194/egusphere-2025-3666
Preprint. Discussion started: 16 September 2025

410 the internal component of member 40 (Fig. 5n) except that both have a patch of cooling in the central tropical Pacific, consistent with the muted warming there in observations (Fig. 5a).

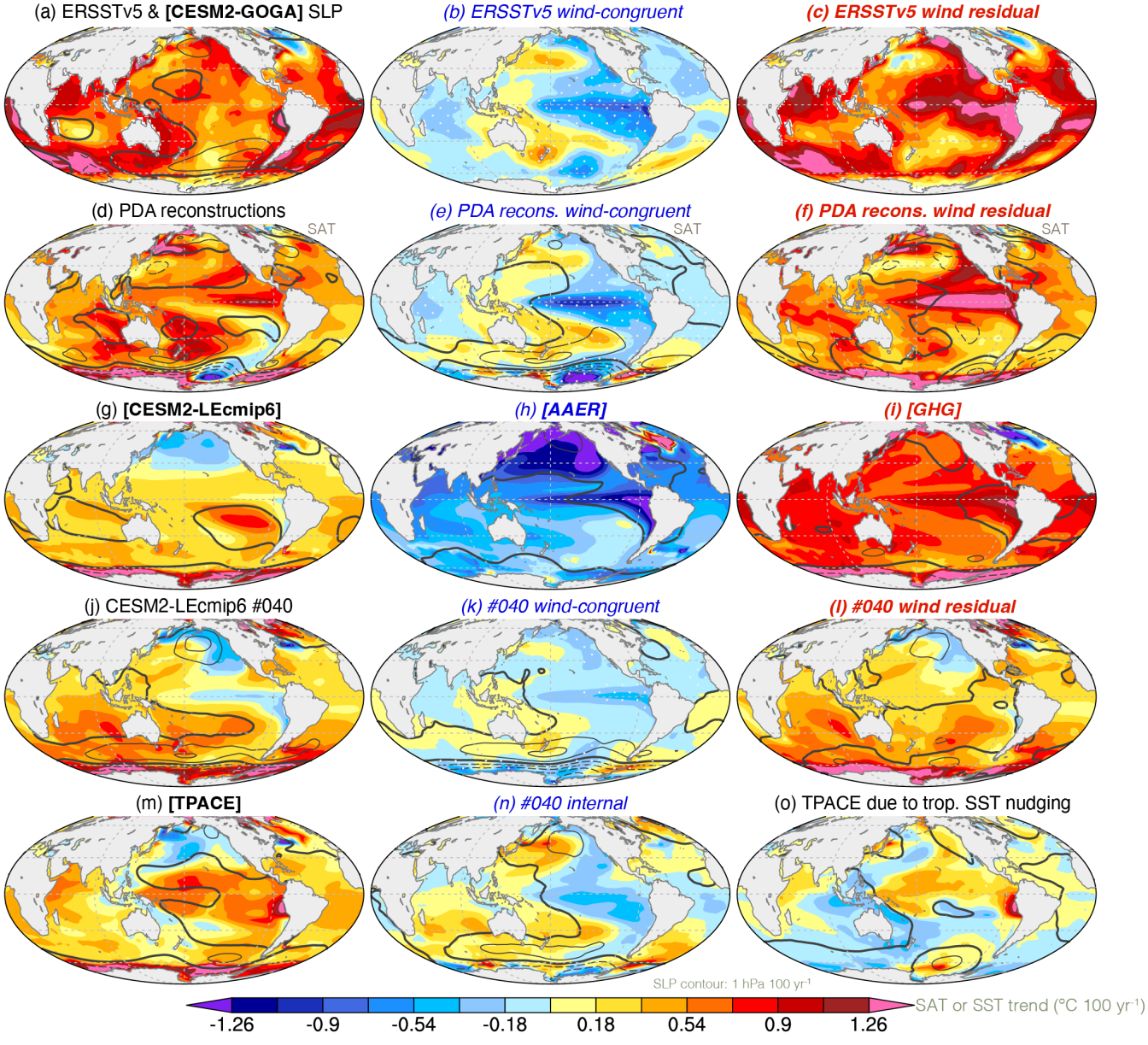

Figure 5. Near-global linear trend patterns (1901-2000) in annual-mean SST (or SAT, as indicated) and SLP in observed, reconstructed, and simulated datasets. In the left column, the original trends are shown without any filtering applied. In the
415 **middle column panels b), e), k), n) the trends congruent with the zonal wind index or associated with internal variability are shown. In the right column panels c), f), l), residual trends after removal of the wind-congruent trends are shown. In the middle row, the forced responses to all forcings in panel g) CESM2-LEcmip6 are compared with responses to aerosols alone in panel h) and greenhouse gases alone in panel i). The SST (or SAT) trends are in °C 100 yr^{-1}. SLP contours (gray lines) are in intervals of 1 hPa 100 yr^{-1}. Negative SLP values are dashed lines and positive values are solid line; the zero contour is a heavier solid line. For**

https://doi.org/10.5194/egusphere-2025-3666
Preprint. Discussion started: 16 September 2025

the PDA reconstructions, CESM1-LE PDA is used for SAT and CESM2-LE PDA is used for SLP and the zonal wind index. Radiative surface temperature is used for the model results in panels g) - o). On the wind-congruent maps, stippling indicates areas where the detrended 50° S - 70° S zonal wind index is significantly correlated at the 95% confidence level or better (using a two-tailed t-test) with the detrended surface temperature anomalies in that location.

In summary, modeling a good fit to the reconstructed accumulation trend pattern requires a) A deepened ASL; b) Stronger circumpolar westerlies; and c) A strong zonal SST gradient in the subtropical Pacific, with more warming in the western than eastern part of the basin. Holland et al. (2022) similarly find that western subtropical Pacific warming accompanies ASL deepening, which they hypothesize is part of a negative IPO-like pattern of internal variability. Consistently, member 40's internal component is a negative IPO pattern. Note that the pattern congruent with reconstructed winds (Fig. 4e) differs from the canonical negative IPO in that it has its strongest loadings in the Amundsen Sea region.

3.3 Recent patterns of change

For 1979-2019, we adopt [CESM2-GOGA] as the reference pattern (Fig. 6a). [CESM2-GOGA] has no trend in the Antarctic-wide accumulation rate, consistent with results from reanalysis and regional models (e.g. Clem et al., 2023; Mottram et al., 2021). Like the pattern during the twentieth century, a trend dipole occurs across the WAIS, consistent with the deepened ASL (Fig. 1a). Negative accumulation trends occur in Wilkes Land, where the thinning Totten Glacier is located and in West Antarctica over the thinning Thwaites and Pine Island glaciers (e.g., Shepherd et al., 2019). The trend magnitudes are weaker in [CESM2-TOGA] (Fig. 6b), which does not simulate the negative trend over Totten. This suggests that regional accumulation trends are responsive to extratropical SST and sea ice trends, consistent with mid-to-high latitude moisture sources of Antarctic precipitation (Sodemann and Stohl, 2009).

The coupled experiments, [CESM2-LEcmip6] (Fig. 6c) and [TPACE] (Fig. 6d) exhibit strong upward accumulation trends, inconsistent with observations. Spatially, [TPACE] fits the reference pattern given by [CESM2-GOGA] better than does [CESM2-LEcmip6]. Although tropical pacemaker experiments can simulate ASL deepening for the period since 1979, they do not simulate Antarctic sea ice expansion and Southern Ocean surface cooling (Schneider and Deser, 2017), which explains why [TPACE] simulates too strong of an accumulation trend. A temporal perspective on these recent trends is provided in Figure 6e. In MT19 and the prescribed SST experiments, most of the accumulation increase occurs between about 1970 and 1990, during a period of Southern Ocean warming (Zhang and Deser, 2024). In the coupled experiments, the accumulation rate steadily increases from about 1970 through the end of the timeseries.

https://doi.org/10.5194/egusphere-2025-3666
Preprint. Discussion started: 16 September 2025

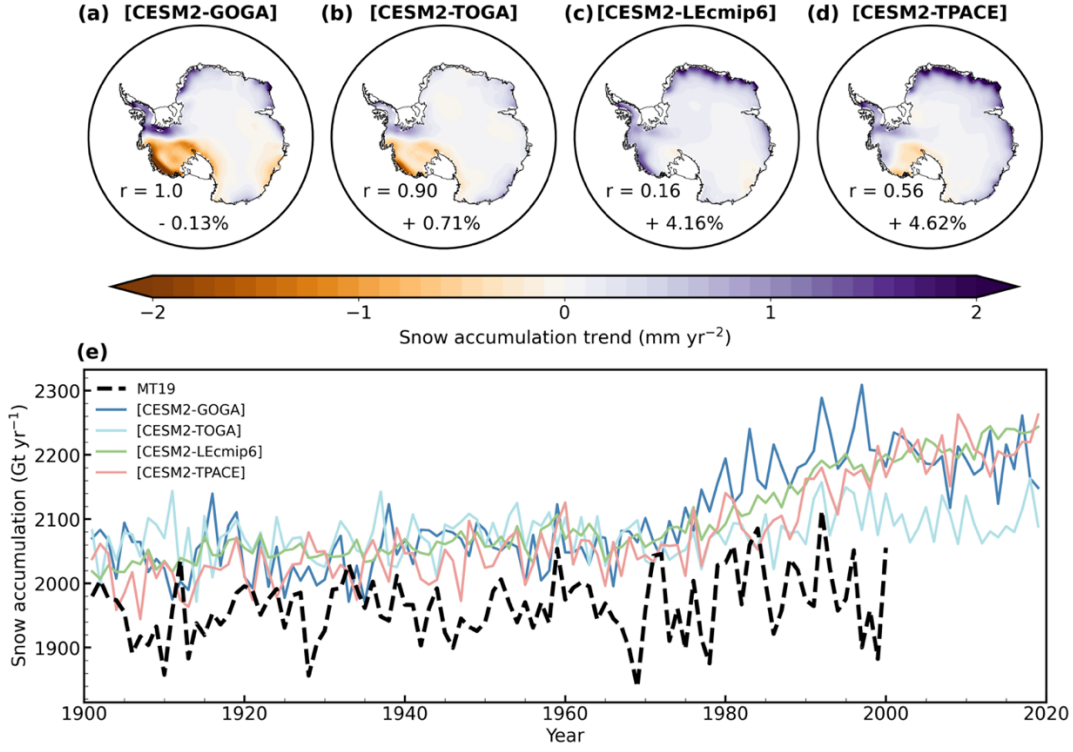

Figure 6. Maps of 1979-2019 linear trends in snow accumulation for a) [CESM2-LEcmip6], b) [CESM2-TPACE], c) [CESM2-TOGA], and d) [CESM2-GOGA]. The percentages indicate changes of the Antarctic-wide snow accumulation rate averaged over 2005-2019 compared with 1979-1993. The r values represent the pattern correlation of the simulated trend with the trend given by [CESM2-GOGA]. e) Timeseries of annual snow accumulation over the grounded AIS from MT19 and various model simulations.

The ASL has continued to deepen in the twenty-first century (Fig. 1a), as reflected in the 2001-2022 SLP trend pattern in ERA5 (Fig. 7a). The ASL deepening is embedded within a larger-scale trend pattern associated with the positive phase of the SAM. The ERA5 SLP and snow accumulation patterns are well captured in CESM2-WNUDGE (Fig. 7b). Underlying the nudged pattern is a steady upward trend in the forced response (Fig. 7c) associated with background warming. Figure 7d isolates the effect of the wind nudging, which drives cooling in the Amundsen Sea but strong warming in the western Ross Sea, reminiscent of the pattern associated with wind-congruent trends in the reconstructions (Fig. 4e). Generally, the predominant trend pattern of the twentieth century has continued into the twenty-first century.

Large-scale orographic effects are evident in the wind-driven accumulation pattern. The WAIS divide separates the positive and negative snow accumulation trends, with Elsworth Land on the windward side and Marie Byrd Land on the lee side with respect to the ASL. In East Antarctica, Queen Maud Land receives high snowfall as it faces the winds, and its climatological moisture transport pathway (Nakka et al., 2021) is enhanced by the trend pattern. The positive snow accumulation trend extends inland to the South Pole, qualitatively consistent with observations there (Zhai et al., 2023). At least

https://doi.org/10.5194/egusphere-2025-3666
Preprint. Discussion started: 16 September 2025

some of the increased cyclonic activity in the Amundsen Sea and south Atlantic, associated with positive snow accumulation trends in the Peninsula region and Queen Maud Land, respectively, is driven by the forced response (Fig. 7c). A negative snow accumulation trends occurs across most of the terrain that lies downwind of the main East Antarctic ice divide. The largest negative trends occur in Wilkes Land. A recent observational study (Wang, Ma et al., 2025) found a significant decrease in the 2005-2020 accumulation rate along a transect from Zhongshan Station (69° S, 76° E) to Dome A (80° S, 77° E), associated with trends in the large-scale atmospheric circulation and consistent with the accumulation trend pattern in CESM2-WNUDGE.

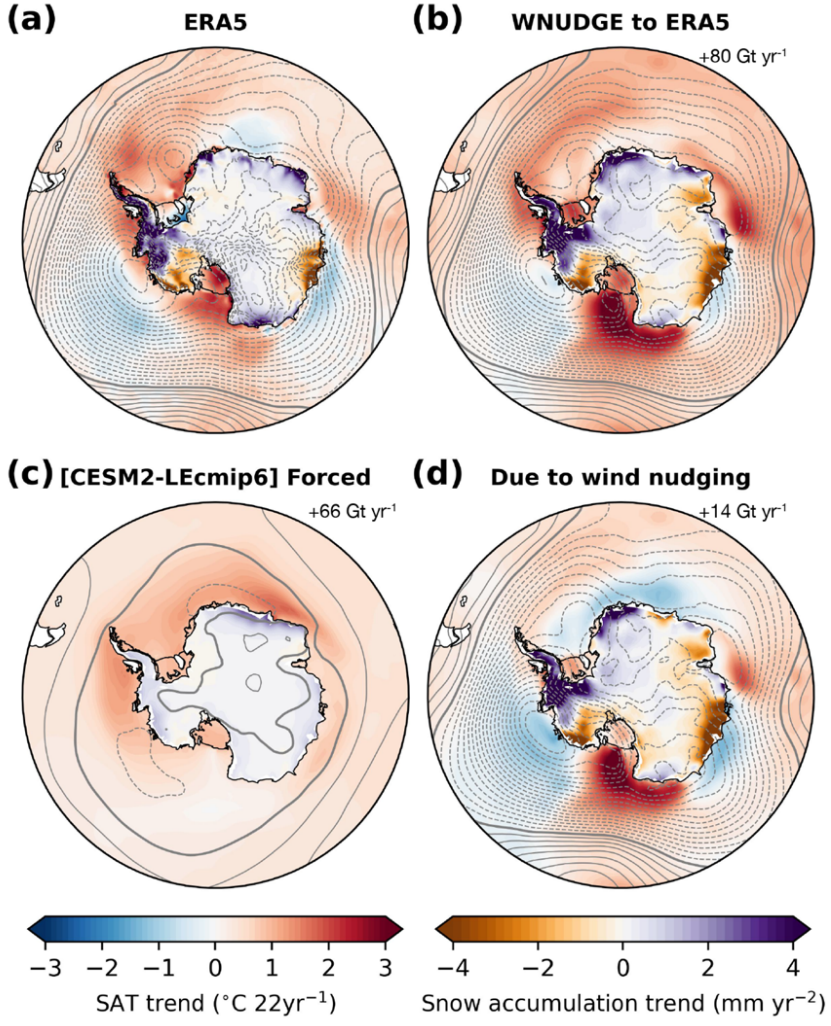

Figure 7. Maps of 2001-2022 linear trends in snow accumulation, SAT and SLP for a) ERA5 (precipitation minus evaporation used to estimate the snow accumulation pattern); b) CESM2-WNUDGE; c) [CESM2-LEcmip6]; d) internal pattern due to wind nudging (forced response from panel c removed). SAT trends are in C 22 yr^{-1}. SLP contours (gray lines) are in intervals of 0.015 hPa yr^{-1}. Negative SLP values are dotted lines and positive values are solid lines; the zero contour is a heavier solid line. Values in the upper-right of b), c), and d) indicate the change in Antarctic-wide accumulation rate for 2019-2022 minus 2001-2005.

https://doi.org/10.5194/egusphere-2025-3666
Preprint. Discussion started: 16 September 2025

3.4 Hidden roles for meltwater and two-way teleconnections

While atmospheric circulation explains spatial accumulation patterns, temperature in and around Antarctica is the main driver of the accumulation rate. The most pronounced period of Southern Ocean surface cooling and increasing sea ice extent in recent years was 1980-2013, which corresponds with the period covered by the meltwater experiment. For comparison, we include [CESM2-GOGA] (Fig. 8a) and the older [CESM1-GOGA] (Fig. 8b), which uses the same CAM5 atmospheric model as [CESM1-AIS meltwater] (Fig. 8c). The meltwater experiment was designed to represent the spatial pattern of freshwater fluxes from ice shelf basal melt, with the total magnitude of these fluxes set to 2000 Gt yr^{-1} to force the model to significantly reduce its rate of sea ice loss relative to the CESM1 Large Ensemble (Pauling et al., 2016). The snow accumulation pattern in the meltwater experiment exhibits good agreement with the pattern in [CESM1-GOGA] (r = 0.62), while having a less than 1% increase in the Antarctic-wide accumulation rate during 1979-2013.Thus, the accumulation response to meltwater is consistent with the response to the observed SSTs.

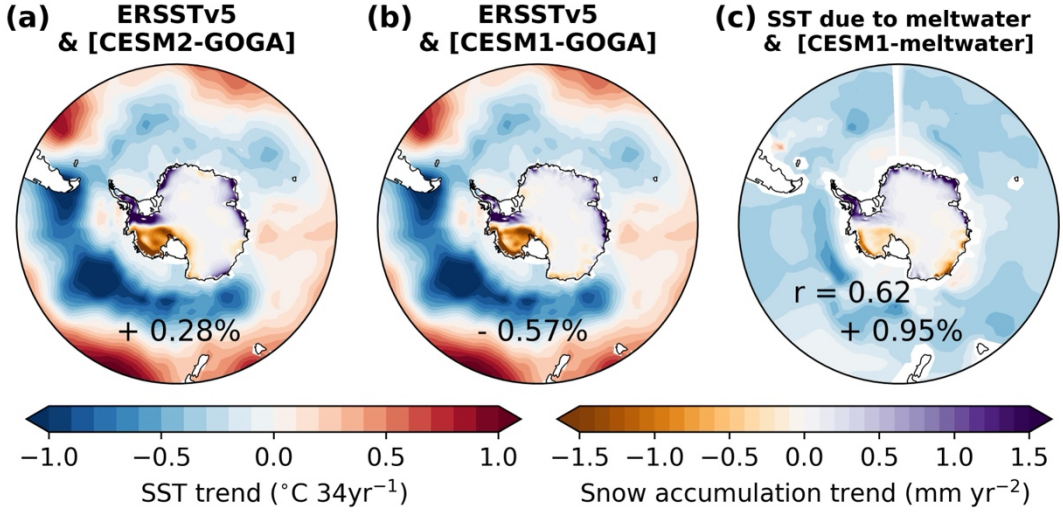

Figure 8. Maps of 1980-2013 linear trends in snow accumulation and SST for a) [CESM2-GOGA] and ERSSTv5; b) [CESM1-GOGA] and ERSSTv5 ; c) [CESM1-AIS meltwater], with the SST trend due to meltwater hosing (forced response from CESM1-LE removed; see Armour et al. (2024) for SSTs with the radiatively forced response included). Also shown is the percentage change in the Antarctic-wide accumulation rate between the averages of (2000:2013) and (1980:1993), as well as the pattern correlation of [CESM1-AIS meltwater] with [CESM1-GOGA]. The CESM1-GOGA ensemble prescribed ERSSTv4 but ERSSTv5 data are displayed here for illustration purposes.

As discussed in previous work (Dong et al. 2022a; Armour et al., 2024), Antarctic meltwater reduces global-mean warming and reduces effective climate sensitivity via the SST pattern effect. Since

https://doi.org/10.5194/egusphere-2025-3666
Preprint. Discussion started: 16 September 2025

accumulation responds to temperature, it follows that meltwater reduces accumulation. A key piece of the SST pattern effect is the zonal SST gradient in the subtropical south Pacific, which CMIP6 models systematically do not replicate (Wills et al., 2022). In the reconstructions for 1901-2000, there is less warming in the subtropical and mid-latitude eastern Pacific than in the western part of the basin even if the wind-congruent trends are removed (Fig. 9a). This is a stronger gradient than can be explained by GHGs alone (Fig. 5i), suggesting that another signal is present. The meltwater-induced pattern (Fig. 9b) could be this missing signal, as it features more cooling in the eastern than western Pacific. If the meltwater signal is added to [GHG], the resulting pattern (Fig. 9c) is strongly correlated ($r = 0.91$ over 30°S-70°S) with the wind-residual pattern in the PDA reconstruction (Fig. 9a).

To scale the meltwater anomaly pattern in Figure 9b, we multiply the decadal meltwater-induced trend estimated by Dong et al. (2022a) by five. This is justified on the grounds that ice shelf thinning and grounding line retreat in West Antarctica commenced in the mid-twentieth century, several decades prior to the modern satellite era (Smith et al., 2017; Clark et al., 2024), contributing anomalous freshwater to the ocean. Prescribed SST simulations indicate that from the mid-twentieth century onwards, stabilizing cloud feedbacks have damped global warming (Andrews et al., 2022). In snow accumulation, it is around 1950 when the cumulative mass gain in [CESM2-LE] begins to outpace the gain in the MT19 reconstruction (Fig. 2a), and when the signal in [TPACE] noticeably counteracts the signal in [CESM2-LE*] (Fig. 2c). It is plausible that a meltwater-driven cooling signal could be propagated towards the subtropics via atmospheric advection and a chain of wind-SST-cloud feedbacks (Dong et al., 2022a, 2022b; Kim et al., 2022; Kang et al., 2023) and be embedded in the observed SST record and the proxy records. ERA5 trends over 1950-2024 show cooling around 60° S, 180° W (Fig. D1) that is consistent with the meltwater response in Figs. 9b-9c. The pattern due to tropical SST nudging in TPACE (Fig. 9d) shows a central Pacific El Niño- like state (resembling "El Niño Modoki" e.g. Ashok et al., 2009) that is consistent with the response to meltwater (Fig. 9b). Note that it is the previously discussed wind-congruent portion of the SST and SLP trends that are associated with the strengthened Walker Circulation.

https://doi.org/10.5194/egusphere-2025-3666
Preprint. Discussion started: 16 September 2025

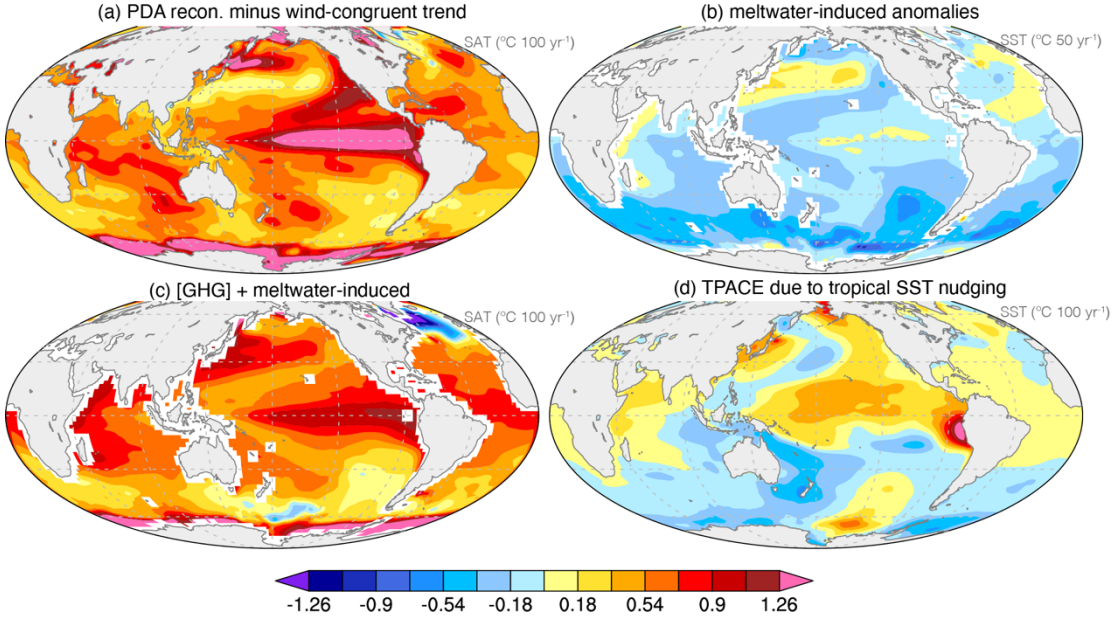

Figure 9. a) Map of 1901-2000 trend in CESM1-LE PDA SAT after removal of the wind-congruent trends (as in Fig. 5g); b) SST anomalies due to historical Antarctic meltwater anomalies from the CESM1-AIS meltwater experiment (decadal trend multiplied by five to estimate meltwater's role over the second half of the century); c) SST anomalies formed from [GHG] (as in Fig. 5i) added to the meltwater-induced anomalies in panel b. d) 1901-2000 trend in TPACE due to tropical SST nudging. To ensure that the anomalies in d) are not aliasing interannual ENSO variability, an 8-y lowpass filter was applied to annual timeseries in [TPACE]-[CESM2-LE*] before computing the trend. We suspect that the strong positive trend in the far eastern equatorial Pacific is an artifact of observational uncertainties in the ERSSTv5 dataset. Over 30° S - 70° S, the wind-residual anomalies in panel a correlate with the anomalies in panel c at r = 0.91. Radiative surface temperature is used for [GHG]. Note that the SAT pattern in a) likely contains an aerosol signature, especially in the north Pacific and north Atlantic.

3.5 Reconciling the reconstructed and modeled trends in cumulative mass

The preceding results offer a physical basis for adjusting the cumulative mass timeseries from MT19 to bring it in agreement with the responses in the Large Ensemble and TPACE. We use the accumulation vs. wind regression coefficient from Fig. 4e multiplied by the trend in the wind index, to estimate how much mass gain or loss would have happened without the dominant pattern of climate variability that has occurred in the real world. The adjustment applied agrees closely with the response to SST nudging in TPACE while removing this signal from the original MT19 timeseries brings the reconstruction and [CESM2-LEcmip6] into agreement with each other (Fig. 2c). While this close fit in part arises from the dynamical consistency of CESM2-LEcmip6 and CESM2-LE PDA (which includes proxies from MT19), the linkage between winds (or SAM) and Antarctic accumulation has been verified across multiple reanalysis datasets (Medley and Thomas, 2019; see Appendix A). The integrated SAM (and lagged ENSO) history explains gravity and ice sheet height anomalies due to Antarctic surface mass balance anomalies (King and Christoffersen, 2024).

The interpretation of the anomalies due to SST nudging in TPACE is challenging (Fig. 9d). Nominally, the forced response of the westerly winds driven by stratospheric ozone depletion and greenhouse gases

https://doi.org/10.5194/egusphere-2025-3666
Preprint. Discussion started: 16 September 2025

is removed in differencing [TPACE] and [CESM2-LE*]. There could be biases in the response to winds, as suggested by the weak wind-congruent SST anomalies in member 40 (Fig. 5k), despite the simulated wind trend itself being in good agreement with the wind history constrained by CESM2-LE PDA (Fig. 2b). It is difficult to explain the nudged SST pattern by internal variability, as there is a strong consensus that the internal variability pattern that fits observations is the negative phase of the IPO; the nudged SST pattern is roughly opposite to negative IPO. As discussed above, there is an argument to be made that the nudged SST pattern fits the response to meltwater, but the magnitude of meltwater forcing since the mid-twentieth century is difficult to constrain. We add that the responses to SST nudging in TPACE in both SLP and SST (Fig. 5o) are similar to the "Pattern 2" described by Wills et al. (2022) that captures the difference between observed and modeled SST and SLP trends. The discussion below highlights how the wind history, meltwater forcing, and internal variability are intimately connected, blurring the distinctions among them. The bottom line is that the wind history constrained by PDA can reconcile differences between observed and modeled trends in Antarctic accumulation as well as surface warming patterns across the Southern Ocean and eastern Pacific.

4 Discussion

4.1 Anthropogenic increase in snow accumulation

The first part of our analysis focuses on attributing the twentieth-century history of Antarctic snow accumulation using the single-forcing large ensemble and the all-forcings Large Ensemble from CESM2. We evaluate what combination of external forcing and internal variability explains the historical trends and therefore may be applied towards more accurate projections of snow accumulation into the future. Greenhouse gases have been the primary driver of increased snow accumulation on the AIS, leading to a cumulative mass gain of 21 mm SLE for 1901-2000 due to their role in warming the atmosphere and ocean surface. Internal variability over the twentieth century cannot explain the observed cumulative mass gain, but internal variability could combine with the forced response to greenhouse gases and aerosols (when used together in the same Large Ensemble experiment) to reduce the magnitude of the cumulative mass gain. This contrasts with Previdi and Polvani (2016), who argue that internal variability has completely masked the anthropogenic increase in Antarctic snow accumulation. Their study did not have the long observational perspective of the MT19 reconstruction to work with, nor the single-forcing large ensemble. By employing these datasets and applying the cumulative mass gain metric, the anthropogenic signal in snow accumulation can be detected.

https://doi.org/10.5194/egusphere-2025-3666
Preprint. Discussion started: 16 September 2025

610

Table 2. 1901-2000 cumulative mass gain from increased snowfall on the AIS in MT19 and various CESM2 experiments (standard deviation arises from the ensemble spread). Right column summarizes the interpretation discussed in the text.

	Cumulative mass gain	Summary interpretation
MT19	3824 ± 1046 Gt	response to greenhouse-gas driven warming, offset by SST trends associated with winds and meltwater, with small offset role for aerosols
[CESM2-LEcmip6]	6434 ± 1242 Gt	combined response to all forcings, with biased response to biomass burning aerosols, but meltwater missing
[CESM2-LE]	6079 ± 1186 Gt	combined response to all forcings, with corrected biomass burning forcing, but meltwater missing
[TPACE]	4167 ± 855 Gt	combined response to all forcings, the tropical response to Antarctic wind and meltwater, and Antarctic response to tropically induced Rossby waves
[AAER]	-3156 ± 960 Gt	mass loss arising from aerosol-driven cooling that is too strong due to spurious Antarctic sea ice - albedo feedbacks
[GHG] **[GHG] + [AAER]**	7483 ± 1220 Gt 4185 ± 2231 Gt	response to greenhouse gases, plus too-strong aerosol response that approximates the responses to aerosols and meltwater combined
[EE]	745 ± 1293 Gt	mass gain largely due to late-twentieth century stratospheric ozone depletion but with other influences

615 Table 2 summarizes our interpretation of the cumulative mass gain results, and how a missing meltwater forcing in conjunction with a "reverse" tropical teleconnection could reconcile results among the experiments and the reconstructions. What this does not resolve is the portion of the wind-congruent accumulation trends that are attributable to external forcing vs. internal variability, nor the question of whether West Antarctic ice shelf thinning (the source of the meltwater forcing) was naturally triggered.
620 These questions are explored in Holland et al. (2022). From their study, the pattern of internal variability that fits PDA-reconstructed atmospheric circulation trends is the negative phase of the IPO, which concurs with our analysis. However, the pattern we uncover differs from the canonical IPO pattern (which resembles the internal pattern in member 40, Fig. 5n) in that it is not symmetrical about the equator; it has stronger loadings in the Southern Hemisphere. The ASL is part of the negative IPO
625 pattern; Dalaiden et al. (2024) attribute ASL deepening trends to a combination of IPO variability and anthropogenic forcing. Holland et al. (2022) suggest that the mid-to-late twentieth century strengthening of the westerlies is attributable to anthropogenic forcing. They also suggest that while ice-shelf thinning may have been naturally triggered in the mid-twentieth century, it has been sustained by anthropogenic forcing.

630

Results presented here agree with the previous attribution work. Much of the reconstructed circulation trend can be explained by the forced responses to greenhouse gases and "everything else" but there is considerable spread across the Large Ensemble arising from internal variability (Fig. C4). The ensemble member that best matches the reconstructed circulation history and accumulation spatial pattern,
635 member 40, does not exhibit the strong relationship between winds and surface temperature trends that is evident in reconstructions and observations (Figs. 4, 5). This decoupling has major consequences for

https://doi.org/10.5194/egusphere-2025-3666
Preprint. Discussion started: 16 September 2025

the simulated Antarctic-wide accumulation rate and the corresponding SST trends. It suggests either misrepresented processes or a missing forcing.

4.2 SSTs (and sea ice) explain lack of 1980 to near-present accumulation trend

In the context of anthropogenic warming, the lack of an observed increase in Antarctic-wide accumulation for 1980 to near present has been puzzling. Surface cooling (or muted warming) of the Southern Ocean is the solution to this puzzle. In a prescribed SST and sea ice experiment, CESM2-GOGA, no trend in the Antarctic-wide accumulation rate occurs, in contrast to the coupled Large Ensemble in which accumulation steadily increases. In the coupled CESM1, the snow accumulation trend is reduced by prescribing ice shelf meltwater fluxes. Qualitatively similar results are obtained from a CESM2 experiment nudged to observed Southern Ocean SST anomalies (Fig. C6; Kang et al., 2023). Not only do these constrained experiments reduce the overall accumulation rate, they also better resolve the regional pattern of snow accumulation trends than does the Large Ensemble. Other studies have used the same or similar experiments to explain the SST pattern effect, with a focus on SST trends in the tropical and subtropical eastern Pacific (Kang et al., 2023; Dong et al., 2022a; Armour et al., 2024; Zhang and Deser, 2024).

4.3 Aerosol and tropical pacemaker experiments together support a role for meltwater

Over the twentieth century, the agreement of the cumulative mass gain in [TPACE] and [GHG] + [AAER] is striking. They agree because they are both associated with reduced Southern Ocean warming (relative to the forced response in the all-forcings Large Ensemble), consistent with the mechanism discussed in the preceding paragraph. As diagnosed by Simpson et al. (2023), positive ice-albedo feedbacks in [AAER] act on a cold pre-industrial background state, leading to strong cooling. These feedbacks are not as pronounced in [CESM2-LE] in which aerosols are introduced only after the climate has warmed somewhat due to increasing greenhouse gases. The strong cooling in [AAER] is artificial, but instructive to the mechanism that explains reduced accumulation. From an Antarctic-wide perspective, it does not matter that cooling in [AAER] is maximized in the Atlantic and Indian Ocean sectors rather than in the Pacific sector (Fig. 5h). Similarly, relative cooling in TPACE is maximized in the Indian Ocean sector (Fig. 5o). However, these patterns do not fit what actually has happened in the twentieth- and early twenty-first centuries - relative cooling has been maximized in the Pacific sector (Fig. 4a).

In member 40, the negative IPO SST pattern in conjunction with the ASL deepening trend, results in the correct pattern of snow accumulation, but there is virtually no reduction in the Antarctic-wide accumulation rate relative to the forced response. The reconstructions reveal that cooling was maximized in the Amundsen Sea Embayment, and that this cooling trend is linked with SST trends in the tropical Pacific. The Amundsen Embayment is precisely the region where ice shelves have been thinning since the mid-twentieth century (Clark et al., 2024), and of course meltwater fluxes from ice shelves are not included in the Large Ensemble and other similar experiments. The amplified response to a forcing perturbation in [AAER] suggests that even if these anomalous freshwater fluxes were

https://doi.org/10.5194/egusphere-2025-3666
Preprint. Discussion started: 16 September 2025

relatively small, this signal would have been amplified by strong sea ice albedo and shortwave cloud feedbacks. The forced response of [CESM2-LE] plus IPO-like internal variability is essentially what Holland et al. (2022) say drives the history of Antarctic wind which in turn drives West Antarctic ice shelf basal melt (see also O'Connor et al., in press). The snow accumulation history reveals that meltwater should be added to the equation to explain observed climate trends since 1950.

4.4 Towards constrained future projections

Accurate projection of future changes in snow accumulation is hampered by uncertainty in the evolution of SST trends. To tentatively project potential sea level mitigation from increased accumulation to 20250, we use the lower bound of the GHG + AAER ensemble at 2050 in reference to the value given by [GHG] + [AAER] at the year 2000 (Fig. 10d-e). This is based on the idea that [AAER] has too strong of a cooling and effectively does the work of both aerosols and omitted meltwater to suppress the GHG-driven accumulation increase. Recognizing that aerosol forcing weakens during the twenty-first century while meltwater is likely to increase, we use the 5% lower bound at 2050, giving an average rate of 0.5 mm yr^{-1} of snowfall-related sea level mitigation. As this projection approximates the role of meltwater, we present it for illustration purposes only. In any case, 0.5 mm yr^{-1} is less than the widely used CESM2 Large Ensemble projects, and less than the ice sheets' current rate of contribution to sea level rise (Stokes et al., 2025). If meltwater continues to dampen surface warming (Sadai et al., 2020) snow accumulation will have a hard time keeping up with ocean-driven dynamic mass loss. While the uptick in intense atmospheric river events, recent sea ice loss and warm Southern Ocean conditions could indicate that increased snow accumulation will provide significant sea level mitigation, strong warming will mean more mass lost to surface melting and runoff (Gilbert and Kittel, 2021) especially during atmospheric river events (Wille et al., 2025), and some precipitation falling as rain (Vignon et al., 2021). Spatially, the wind and snow accumulation patterns that were dominant in the recent past should continue, marked by relatively more snow in the Peninsula and Queen Maud Land, and relatively less snow in Wilkes Land and a positive SAM pattern in the pressure field (Fig. 10a-c).

https://doi.org/10.5194/egusphere-2025-3666
Preprint. Discussion started: 16 September 2025

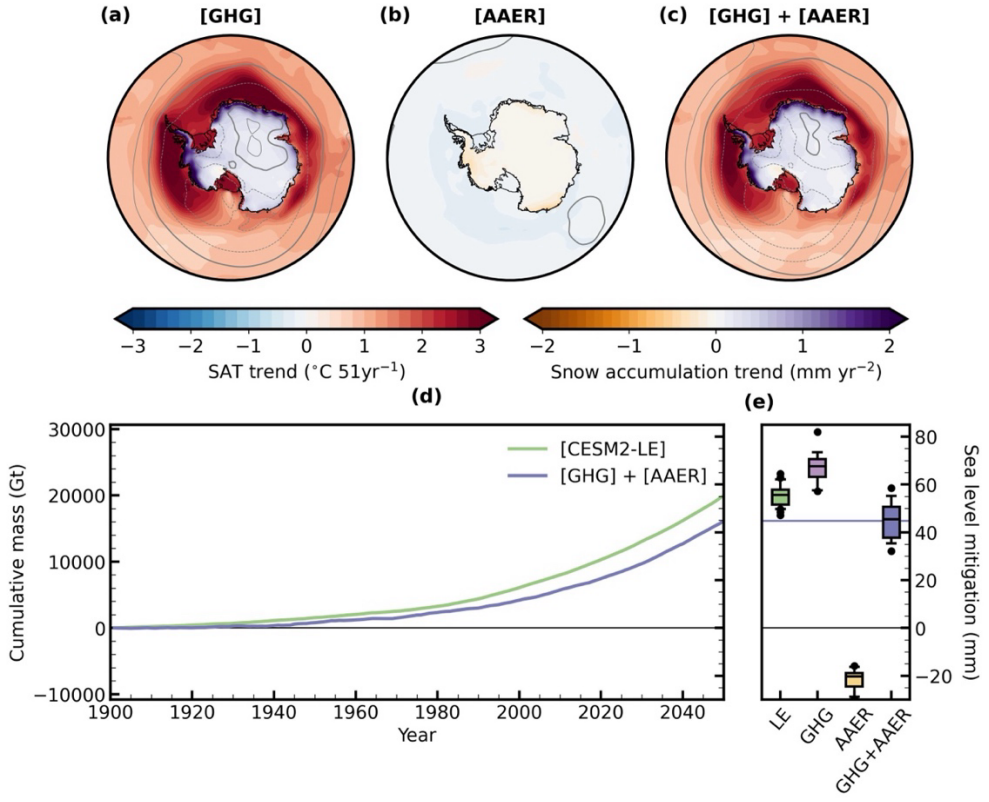

Figure 10. Linear trends in snow accumulation, SLP and SAT during 2000-2050 for a) [GHG]; b) [AAER]; c) [GHG] + [AAER]. SLP contours (gray lines) are in intervals of 0.015 hPa yr^{-1}. Negative SLP values are dotted lines and positive values are solid lines; the zero contour is a heavier solid line. d) Cumulative mass timeseries like in Fig. 2a, but timeseries are extended to 2050. (e) Box-whisker plot like in Fig. 2b, but for mass accumulated over 1901-2050, relative to the piControl baseline. By comparison with Fig. 1b, this indicates that [GHG] + [AAER] projects ~ 28 mm of sea level mitigation over 2001-2050, or an average rate of 0.56 mm yr^{-1}. Applying the 5% lower bound of the GHG + AAER ensemble at 2050 (to account for stronger meltwater/weaker aerosol forcing than in the twentieth century), there would be ~ 23 mm of sea level mitigation during 2001-2050, continuing from ~ 12 mm for 1901-2000, or an average rate of ~ 0.5 mm yr^{-1}.

4.5 Limitations and future work

Higher resolution modeling might change some details of our results and the relative importance of meltwater and winds, but should not change our overall interpretation. Regional high resolution would resolve finer details of the orographic patterns in accumulation, better represent snowfall in coastal regions and may change the response of processes like surface melting to warming (Datta et al., 2023; Noël et al, 2023; Yin et al., 2025). Regional atmospheric grid refinement over the recent historical period in an atmosphere-only configuration produces differences in the simulated snow accumulation conforming strongly to topography and enhanced moisture transport (Datta et al., 2023). Global high resolution enhances the linkage of the Southern Ocean with the tropical Pacific (Chang et al., 2020;

https://doi.org/10.5194/egusphere-2025-3666
Preprint. Discussion started: 16 September 2025

Yeager et al., 2023), which is too weak in most low-resolution models (Chung et al., 2022). The linkage is relatively strong in CESM2 due to its strong shortwave cloud feedbacks (Kim et al., 2022). Low resolution and/or weak shortwave cloud feedbacks could be reasons why CESM1 is not very responsive to meltwater fluxes, requiring a perturbation of 2000 Gt yr^{-1} to produce a significant response (Pauling et al., 2016). Alternatively, if the model's SSTs are more sensitive to winds at high resolution, meltwater may not need to be invoked to explain observation-model discrepancy. Refined regional grids nested within a coarser-resolution global domain (Datta et al., 2023; Yin et al., 2025) and globally high-resolution experiments (e.g. Chang et al., 2020; Yeager et al., 2023) are important tools for future work testing the relative roles of meltwater and winds. Our results imply that the ability of a model to reproduce Antarctic accumulation trends is an important benchmark for any high-resolution experiment that purports to solve observation-model trend discrepancies. Judging from comparison of meltwater and wind-nudged experiments, presented both here and in Armour et al. (2024), it seems that winds alone cannot explain suppressed warming in the Indian Ocean sector, and corresponding decreases in the accumulation rate in Wilkes Land, over the longer record since 1979. Meltwater alone cannot explain the negative IPO-like SST trend pattern across the Pacific.

Observations and/or reconstructions underpin any model evaluation study. We have based our model evaluation on the MT19 reconstruction, which is similar to the kriging reconstruction of Wang and Xiao (2023). Applying two distinct methodologies to the same proxy network, Wang and Xiao (2023) find significant differences between reconstructions. This methodological dependence might be alleviated if more ice core data were available, especially on the East Antarctic plateau (Eswaran et al., 2024) and West Antarctic coastal margin (Neff, 2020). More observations would avoid the need to indirectly infer what trends have occurred in these regions. We have also used CESM2-LE PDA, which is dynamically consistent with the CESM2. Trends in the ERA5 reanalysis qualitatively support the overarching interpretation we have made from these datasets (Fig. D1).

5 Summary and Conclusion

In conclusion, this study bridges the gap between modeled and observed Antarctic snow accumulation trends, with relevance to the failure of models to reproduce SST trends in the Southern Ocean and eastern Pacific (Simpson et al., 2025; Wills et al., 2022). Our results suggest that winds have been working together with ice sheet and ice shelf meltwater fluxes to dampen Southern Ocean surface warming and suppress the GHG-driven snow accumulation increase. In addition, we use the westerly wind history over 50° S- 70° S and its relationship to accumulation to illustrate the linkage between the Southern Ocean and tropical Pacific. The zonal wind index is linearly congruent with SST trends that resemble the pattern most associated with systematic observation-model discrepancies (Wills et al., 2022). While linear congruence does not demonstrate causality, the snow accumulation history seems to suggest this. The strengthening westerlies are associated with reduced snowfall on the Antarctic Ice Sheet, resulting in a cumulative mass loss of ~ 2500 Gt during 1901-2000. This counteracts the forced

https://doi.org/10.5194/egusphere-2025-3666
Preprint. Discussion started: 16 September 2025

response of ~ 6000 Gt by dampening Southern Ocean warming, especially in the Amundsen Sea. The wind-congruent mass loss is close to the ~ 2300 Gt from a model experiment nudged to observed tropical SST anomalies. The wind history is intimately connected with the history of ice shelf thinning and glacial retreat in the Amundsen Sea Embayment (Clark et al., 2024; Holland et al., 2022; O'Connor et al, in press) which initiated during an anomalously warm period in the Antarctic (Schneider and Steig, 2008). In turn, the nudged SST trend pattern in the tropical and subtropical Pacific suggests a role for meltwater, as it is not fully explained by remote forcing from stronger westerly winds. Also, we see little evidence that wind by itself suppresses the Antarctic-wide accumulation rate; its main role is to distribute precipitation unevenly across the continent. Additionally, in contrast to studies emphasizing the role of stratospheric ozone depletion in strengthening the westerlies (e.g. Hartmann, 2022; Dong et al., 2025), the long-term term perspective of paleoclimate data assimilation shows that the strengthening trend (Fig. 1b) began about two decades prior to the onset of the ozone hole, at roughly the same time as ice shelf thinning and glacial retreat in the Amundsen Sea Embayment. To reconcile CESM2's ensemble-mean response with observations, biases in the forced response to winds must be considered along with the omitted meltwater forcing, which itself is a product of internal variability and the forced response. Our overall argument extends the arguments of Roach et al. (2023) about the roles of winds and meltwater on SST trends, of Dong et al. (2022b) about the existence of the Antarctic-to-tropics teleconnection and of Holland et al. (2022) about the internal vs. anthropogenic signals in wind-driven ice shelf basal melt.

Precipitation and other variables from CESM projections are often used to force glacier and ice sheet models with mean-state bias corrections applied, but not with corrections for errors in large-scale SST trend patterns (e.g. Rosier et al., 2025). To place the ~2300 Gt of twentieth-century mass loss attributable to observed SST patterns into perspective, consider that the AIS lost a total of ~ 2720 Gt between 1992 and 2017 when accounting for both dynamic mass loss and changes in surface mass balance input (The IMBIE team, 2018). The CESM2's ensemble-mean version of accumulation increase would have been a welcome addition to the ice sheet's mass. This work underscores a need to keep a model's representation of large-scale warming patterns in mind when downscaling its output, whether for Antarctic studies or projections of climate change in other regions. One path forward is for meltwater to be included in CMIP experiments as a forcing (Sadai et al., 2020; Schmidt et al., 2023). The broader community has been organizing to improve the observational record of meltwater fluxes (Mottram et al., 2024) and to conduct a systematic model intercomparison of the climate response to ice sheet and ice shelf meltwater (Swart et al., 2023; Schmidt et al., 2025). The possible effect of meltwater on snow accumulation raises the urgency of this work. To have a better grasp on Antarctica's role in sea level rise, we encourage many more studies employing different models, experimental designs, and synthesized observational records.

https://doi.org/10.5194/egusphere-2025-3666
Preprint. Discussion started: 16 September 2025

Appendix A: Additional experiments and methods

Table A1. Summary of observationally constrained CESM2 and CESM1 experiments used for evaluation of recent snow accumulation and circulation trends. All experiments use the models at their standard 1° x 1° horizontal resolutions, expect for CESM1-AIS meltwater, which uses a ~ 2° resolution.

abbreviation	model version	radiative forcing	SSTs, sea ice	primary purpose	ensemble members
CESM2-GOGA	CESM2	as in CESM2-LEcmip6; GOGA = 'Global Ocean – Global Atmosphere'	prescribed from ERSSTv5; HadISST1 & OISSTv2 sea ice	find global atmospheric response to observed SST and sea ice anomalies globally	10
CESM2-TOGA	CESM2	as in CESM2-LEcmip6; TOGA = 'Tropical Ocean – Global Atmosphere'	as in GOGA but using climatology polewards of ~28° N and ~28° S	find global atmospheric response to observed SST and sea ice anomalies in the tropics and subtropics	10
CESM2-WNUDGE	CESM2	as in CESM2-LEcmip6; winds nudged to ERA5 55° S-80° S, above 850 hPa	coupled	constrain model to Antarctic winds estimated by reanalysis	1
CESM1-AIS meltwater	CESM1	CMIP5 forcing as in CESM1-LE (Kay et al., 2015) plus Antarctic meltwater hosing	coupled	find atmosphere-ocean response to freshwater fluxes from Antarctic ice shelves	7 for accumulation; 10 for SST
CESM1-GOGA	CESM1	CMIP5 forcing as in CESM1-LE (Kay et al., 2015)	prescribed from ERSSTv4; HadISST1 sea ice	to compare with CESM1-AIS meltwater using the same atmospheric model and radiative forcing	10

Description of observation-constrained experiments

Wind nudging is a technique that can override circulation biases in a model, for example associated with polar stratospheric vortex dynamics (e.g. Gettleman, Mills et al., 2019). In CESM2-WNUDGE the model's winds are nudged to winds from ERA5 (Hersbach et al., 2020) across the middle and high southern latitudes, following a protocol developed with CESM1 (Blanchard-Wrigglesworth et al., 2021) and recently applied to CESM2 (Espinosa et al., 2024). Zonal (U) and meridional (V) winds over January 1950 through November 2023 are nudged to 6-hourly ERA5 U and V from 850 hPa to the top of the model between 55° S and 80° S. The model was free to evolve through the end of 2024. As the first few decades of CESM2-WNUDGE show signs of drift in the Antarctic accumulation values we use only the twenty-first-century portion of this experiment.

Anomalous freshwater fluxes from ice shelves are not included in standard CMIP6 historical experiments nor the experiments in Table 1. Pauling et al. (2016) and Dong et al. (2022a) describe a meltwater hosing ensemble with CESM1 that spans 1980-2013. We utilize this ensemble (using the ensemble mean of 7 members where total anomalous freshwater flux is set to 2000 Gt yr^{-1}, prescribed at the front of ice shelves; we do not consider their surface freshwater experiments) for insight into the

https://doi.org/10.5194/egusphere-2025-3666
Preprint. Discussion started: 16 September 2025

possible influence of meltwater on snow accumulation. A caveat is that the magnitude of the freshwater fluxes imposed in this ensemble are much larger than observational estimates (Pauling et al., 2016).

To directly link Antarctic accumulation with the observed SST and sea ice record, we consider two uncoupled, atmosphere-land-only simulations ("AMIP" style) with prescribed SSTs and sea ice concentrations from observational datasets. The Global Atmosphere - Global Ocean (GOGA) experiment specifies time-varying SSTs and sea ice concentrations throughout the global ocean domain. The Tropical Ocean - Global Atmosphere (TOGA) uses time-varying SSTs in the tropical latitudes only and specifies monthly climatology for SSTs and sea ice concentrations elsewhere.

Snow accumulation and cumulative mass gain calculation

The domain of our snow accumulation calculations is the grounded AIS, as defined by Zwally et al. (2012). Unlike Medley and Thomas (2019), we do not include Antarctic islands in our calculation of Antarctic-wide snow accumulation. For Antarctic-wide snow accumulation from MT19, grid-cell values in mm water equivalent yr^{-1} are scaled by the area of the respective grid cell, and summed over the grounded AIS for each year of the dataset. This mass timeseries is converted to a relative mass timeseries by subtracting the long-term mean for 1801-1900 (1927.4 Gt yr^{-1}) from the entire timeseries. Cumulative mass is calculated by integrating the relative mass timeseries with time, starting in 1901. The sea level equivalence (SLE) at the year 2000 is obtained by dividing the cumulative mass by 361 Gt mm^{-1}. This procedure was repeated for +1 $\boldsymbol{\sigma}$ and -1 $\boldsymbol{\sigma}$ error timeseries; the gridded error fields are as provided by Medley and Thomas (2019) in their MERRA2 reconstruction. Here, the term "relative mass" has a distinct meaning from "Antarctic-wide accumulation rate." Changes in the Antarctic-wide accumulation rate are assessed over specific time intervals, say linear trends over 1901-2000. Relative mass refers specifically to how much the Antarctic-wide snow accumulation rate (expressed in Gt yr^{-1}) in a particular year is anomalous relative to the 1801-1900 baseline value.

From the output of CESM2's land model component, SNOW and RAIN variables are used as the precipitation terms, while QSOIL and QRUNOFF are used as the ablation terms. Monthly data are summed to annual means by weighting each monthly value by the length of the month. The relative and cumulative mass timeseries are determined by the same method as for the MT19 reconstruction, except for the calculation of the preindustrial baseline value.

Crucial for the calculation of cumulative mass and its sea level equivalence from CESM2 is the estimate of the baseline accumulation rate that is representative of nineteenth-century values in a stable climate. We reference each ensemble member to the same baseline value from piControl, averaged over the 452-year period of 1000-1451, yielding 2012.9 Gt yr^{-1}. All ensemble members of all historical experiments in Table 1 had their initial states drawn from this piControl segment, between the years 1001 and 1301, which was chosen because it has a stable control climate (Danbasoglu et al., 2020; Rodgers et al., 2021; Simpson et al., 2023). An ensemble member initialized from the piControl year 1301 at calendar year 1850 would reach calendar year 2000 150 years later, overlapping with piControl through year 1451.

https://doi.org/10.5194/egusphere-2025-3666
Preprint. Discussion started: 16 September 2025

This overlap method is a way of ensuring that mass accumulated by year 2000 arises from forcing (or internal variability), minimizing the influence of drift. The same 1000-1451 piControl period was used for accumulating mass over 24, overlapping 100-yr segments to determine how much mass gain or loss within a century could occur due to internal variability alone, in the absence of anthropogenic forcing.

For the CESM2-GOGA and CESM2-TOGA ensembles, we did not find a representative base period from an uncoupled control integration. Biases in coupled CESM2 SSTs (Danabasoglu et al., 2020) and uncertain nineteenth century observed SSTs (e.g. Huang et al., 2017) further complicate the use of these experiments for cumulative mass in comparison with the Large Ensemble. We therefore use them only to evaluate spatial patterns of change over selected time periods.

Calculating pattern correlations and wind-congruent trends

In evaluating the agreement of simulated and reconstructed trend patterns, we use the pattern correlation metric. Pattern correlations are the Pearson correlation coefficient of the linear correlation between two maps of the same variable. We use the uncentered (no mean value removed) pattern correlation of the trend fields. We calculate trends in snow accumulation, surface temperature, and SLP that are linearly congruent with the trend in the Southern Hemisphere westerly winds as estimated both by the PDA reconstructions and an ensemble member (member 40) of the Large Ensemble. First, the zonal wind index (near-surface zonal wind area-weighted average across 50ºS-70ºS; Fig. 1b) is standardized, while the accumulation, SLP or temperature fields at each grid point are expressed as anomalies relative to 1901-2000. All timeseries, including the wind index and anomaly fields at each grid point are linearly detrended. Then, the linear regression coefficient is calculated between the detrended fields and the detrended wind timeseries. These regression coefficients are multiplied by the 1901-2000 trend in the wind index to give the wind-congruent trends in accumulation, surface temperature or SLP. Residual trends are obtained by subtracting the wind-congruent trends from the trends in the original anomaly fields. The wind adjustment to cumulative mass in MT19 is based on regression of the detrended relative mass timeseries on the detrended, standardized zonal wind timeseries from CESM2-LE PDA. (The gridpoint regression coefficients summed over the continent gives the same result.) The regression coefficient is multiplied by the trend in the wind index to give the slope of the regression line, which is then integrated through time to form the wind-congruent cumulative mass timeseries displayed in Fig. 2c. The wind-congruent cumulative mass timeseries is subtracted from the original MT19 cumulative mass timeseries to give the wind-adjusted MT19 cumulative mass timeseries. Wind-accumulation regressions using 10-m winds from ERA5, or the SAM index of Marshall (2003) are consistent in sign with CESM2-LE PDA but do not exhibit statistically significant correlations with the relative mass timeseries from MT19. Nonetheless, within a given reanalysis framework there are significant relationships between Antarctic accumulation and SAM-related atmospheric circulation indices (Medley and Thomas, 2019).

https://doi.org/10.5194/egusphere-2025-3666
Preprint. Discussion started: 16 September 2025

Appendix B: Verification and comparison of PDA reconstructions

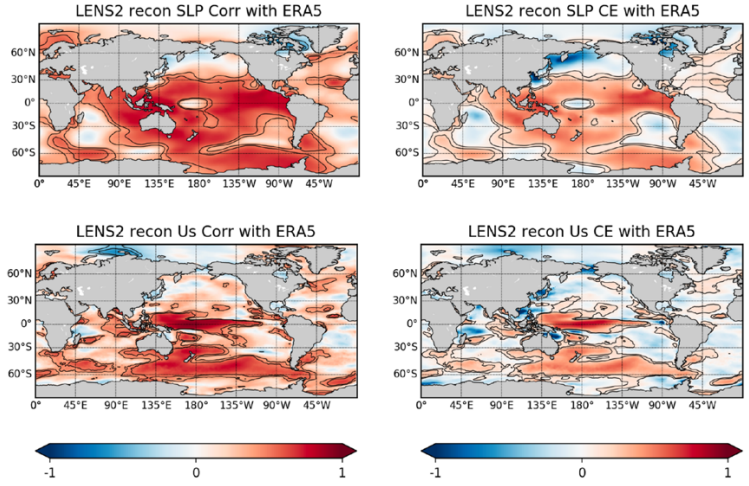

Figure B1. Verification statistics for the CESM2-LE PDA reconstruction SLP (top row) and U10 (bottom row), compared to ERA5 reanalysis for the period of overlap, 1979 to 2005 (anomaly reference period used in this analysis is 1979 to 2005). Correlations are shown on the left, with contours highlighting p-values of 0.01 and 0.05. Coefficient of efficiency (CE) is shown on the right (> 0 demonstrates skill). See further verification and discussion in O'Connor et al. (in press). From https://jortuck.github.io/PaleoclimateVisualizer/, the 50° S - 70° S near-surface zonal wind index that we use from CESM2-LE PDA is correlated with ERA5's zonal winds for 1979-2005 at r = 0.62 (p < 0.01). This wind index is more skillfully reconstructed than the SAM index (O'Connor et al., 2021).

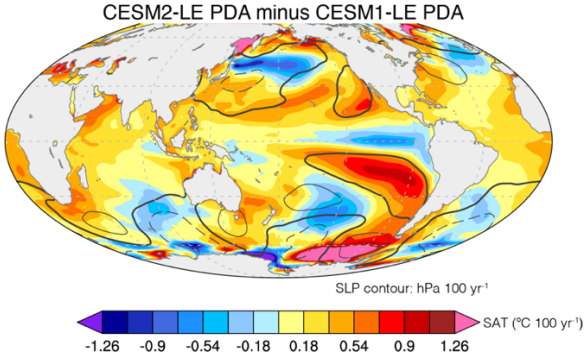

Figure B2: Differences in reconstructed SAT and SLP trends during 1901-2000 between the PDA reconstruction using CESM2-LE as the prior and the reconstruction using CESM1-LE as the prior. For SLP, the dashed black lines represent negative differences, (interval of 1 hPa) the thin solid black lines represent positive differences (interval of 1 hPa), and the zero line is represented by the heavy solid black line. Note the horseshoe-shaped pattern linking the Amundsen Sea region to the eastern subtropical Pacific. We hypothesize that this pattern is primarily caused by shortwave cloud and ice albedo feedback differences between CESM1 and CESM2 (Schneider et al., 2022; Kim et al., 2023), which are extenuated by aerosol forcing (Simpson et al., 2023). Hypothetically, meltwater forcing could make these feedbacks dampen rather than amplify warming.

https://doi.org/10.5194/egusphere-2025-3666
Preprint. Discussion started: 16 September 2025

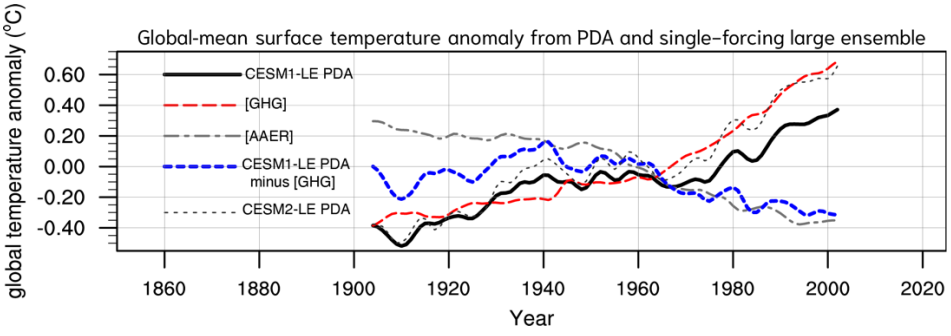

Figure B3: Timeseries of global-mean surface air temperature anomalies during the twentieth century from two different instances of PDA and the ensemble-mean responses in the greenhouse gas and aerosol single-forcing ensembles. All temperature timeseries smoothed with a 7 yr low-pass filter with anomalies relative to 1901-2005;

When twentieth-century SLP trends are subtracted from each other, CESM2-LE PDA exhibits an enhanced zonal wavenumber-3 pattern across the Southern Ocean compared to CESM1-LE PDA (Fig. B2). Figure B2 reveals more noticeable differences in the SAT field. These differences likely arise from different warming patterns in CESM2 vs CESM1 associated with shortwave cloud and surface albedo feedbacks (Schneider et al., 2022), which affect high-latitude atmospheric circulation (Schneider et al., 2020). Given these strong feedbacks, we postulate that with meltwater forcing, the sign of the horseshoe-shaped pattern linking the Amundsen Sea to the tropics would be reversed. This could help reconcile the CESM2-LE PDA global-mean temperature reconstruction with observations, as discussed below. Note that the eastern subtropical Pacific is a region of relatively low skill in the wind and SLP reconstructions (Fig. B1).

In the global-mean (Fig. B3), CESM2-LE PDA warms about 0.2 ºC more than CESM1-LE PDA during the twentieth century. The warming of ~ 0.55 ºC (1976:2000 minus 1901:1925) in CESM1-LE PDA is close to the ~ 0.6 ºC from comprehensive land-ocean datasets like HadCRUT5 (Morice et al., 2021) and GISTEMP (Lenssen et al., 2019). In contrast, global-mean warming in CESM2-LE PDA is almost identical to that in [GHG]. The CESM2-LE PDA apparently disregards information from aerosol forcing in the Large Ensemble, a sign that this forcing may be incorrect and/or there is a missing high-latitude forcing like meltwater. Based on these considerations, we regard the CESM1-LE PDA as the more reliable of the two surface temperature reconstructions, as it is less affected by strong feedbacks that are triggered by aerosol forcing and/or missing meltwater forcing.

https://doi.org/10.5194/egusphere-2025-3666
Preprint. Discussion started: 16 September 2025

Appendix C: Results across members of the Large Ensemble and TPACE, with supporting results from other experiments

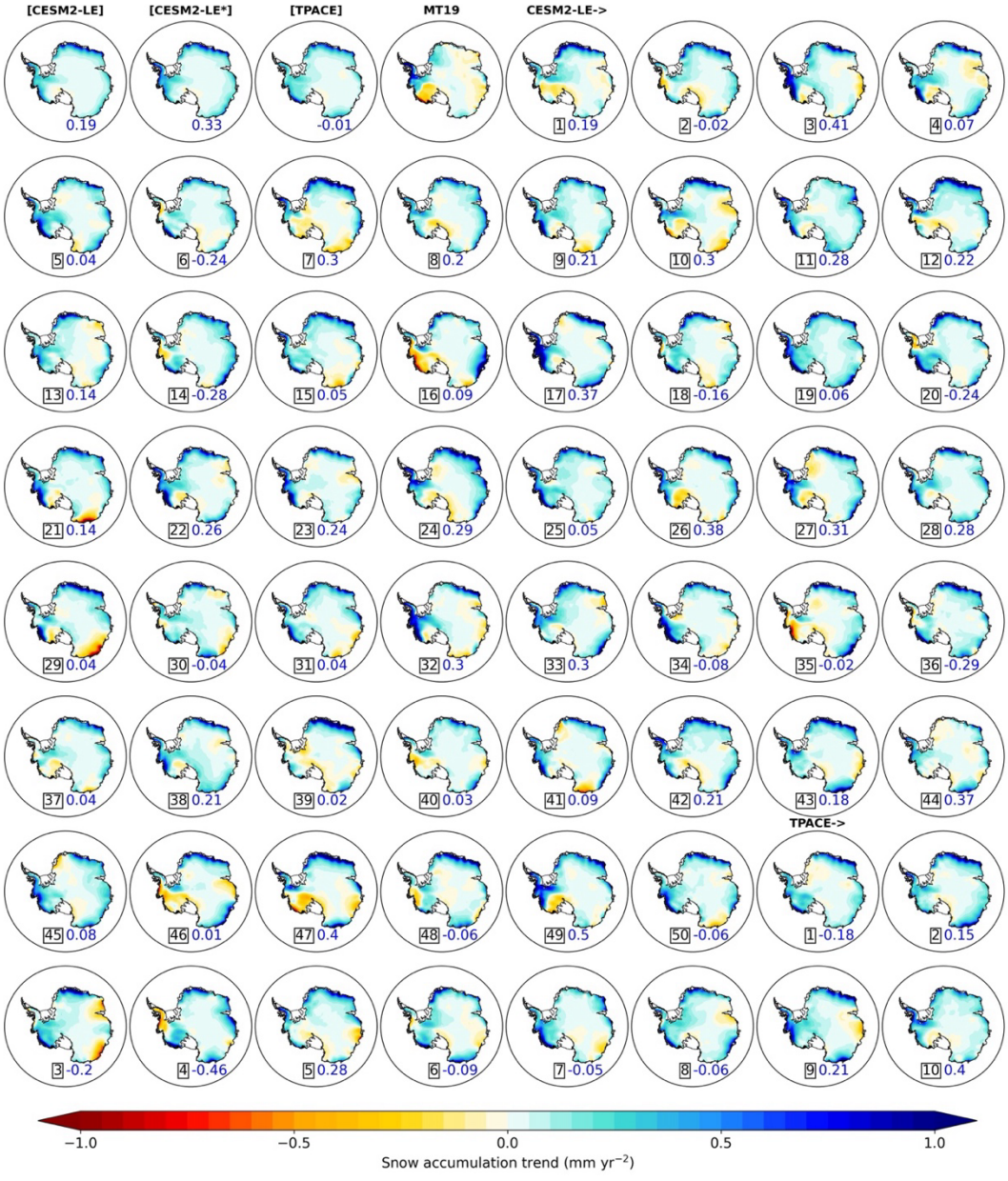

Figure C1. "Postage stamp" maps displaying the twentieth-century snow accumulation (SMB) trend in [CESM2-LE], [CESM2-LE*], and [TPACE], along with all 50 ensemble members of the CESM2-LE and the 10 members of TPACE. Included in the top row is the trend in the MT19 snow accumulation. At the bottom-center of every model map, the spatial pattern correlation coefficient with MT19 over the grounded AIS is shown. Trends are calculated as epoch differences of 1976:2000 minus 1901:1925 annual means.

https://doi.org/10.5194/egusphere-2025-3666
Preprint. Discussion started: 16 September 2025

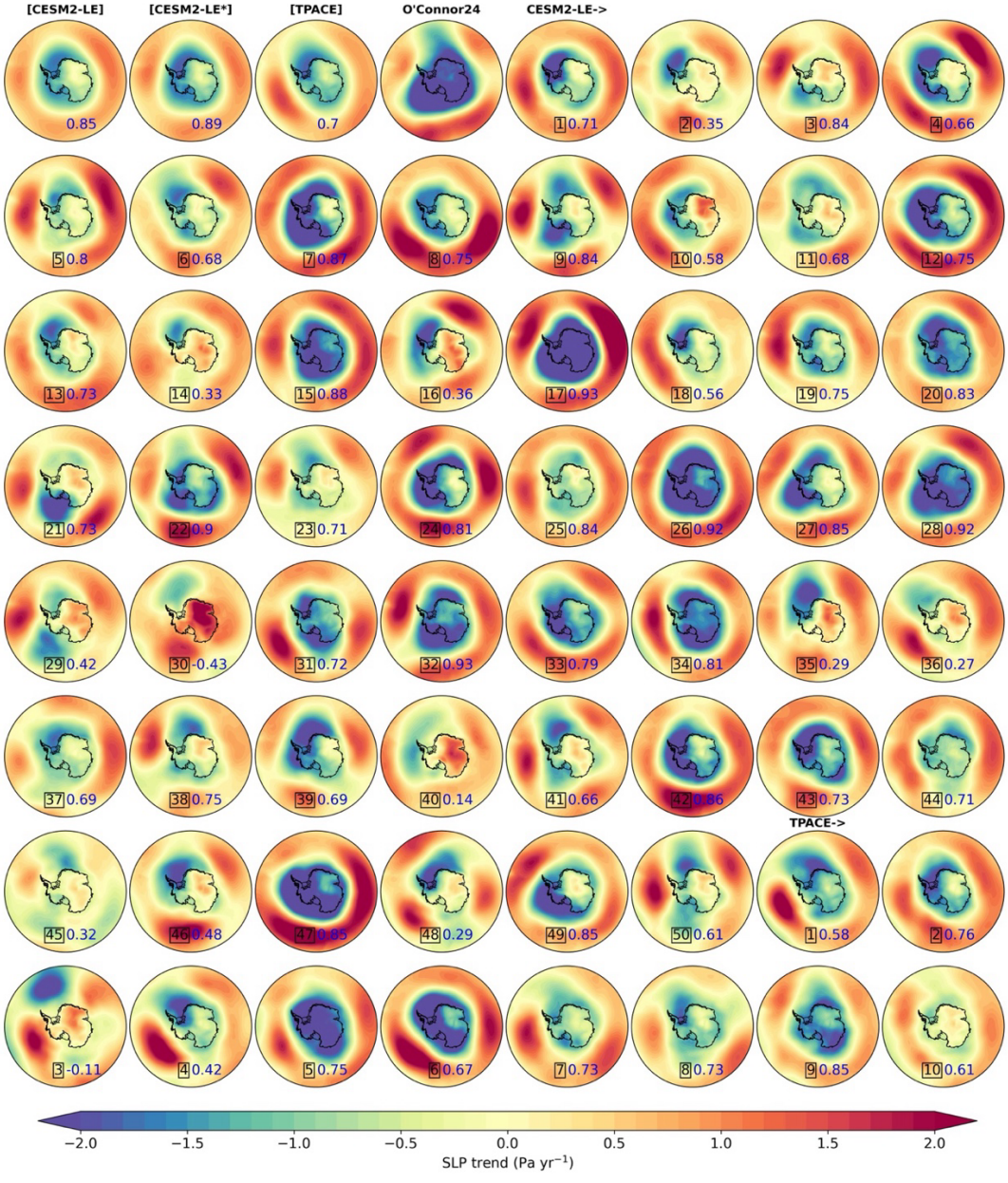

Figure C2: As in Fig. C1, but for SLP and using the CESM2-LE PDA reconstruction (labeled O'Connor24) as the benchmark for the pattern correlation over 40° S - 90°S .

https://doi.org/10.5194/egusphere-2025-3666
Preprint. Discussion started: 16 September 2025

Figure C3. "Postage stamp" maps displaying the twentieth-century snow accumulation (SMB) trend in [CESM2-LEcmip6], [AAER], [GHG], [EE], and [BMB], along with all 50 ensemble members of the CESM2-LEcmip6. Included in the top row is the trend in the MT19 snow accumulation. At the bottom-center of every model map, the spatial pattern correlation coefficient with MT19 over the grounded AIS is shown. Trends are calculated as epoch differences of 1976:2000 minus 1901:1925 annual means.

https://doi.org/10.5194/egusphere-2025-3666
Preprint. Discussion started: 16 September 2025

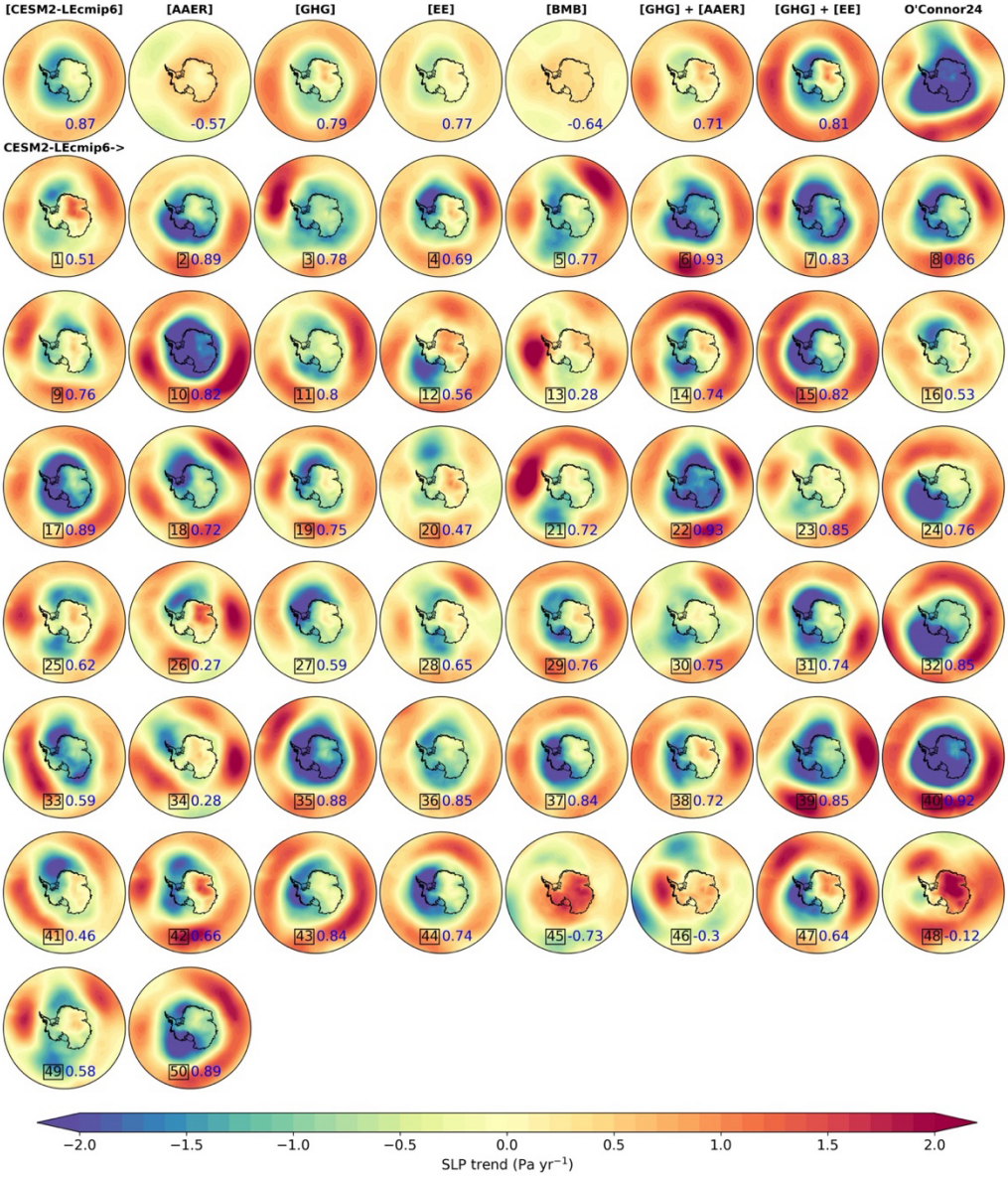

Figure C4. As in Fig. C3, but for SLP and using the CESM2-LE PDA reconstruction (labeled O'Connor24) as the benchmark for the pattern correlation over 40° S - 90° S.

https://doi.org/10.5194/egusphere-2025-3666
Preprint. Discussion started: 16 September 2025

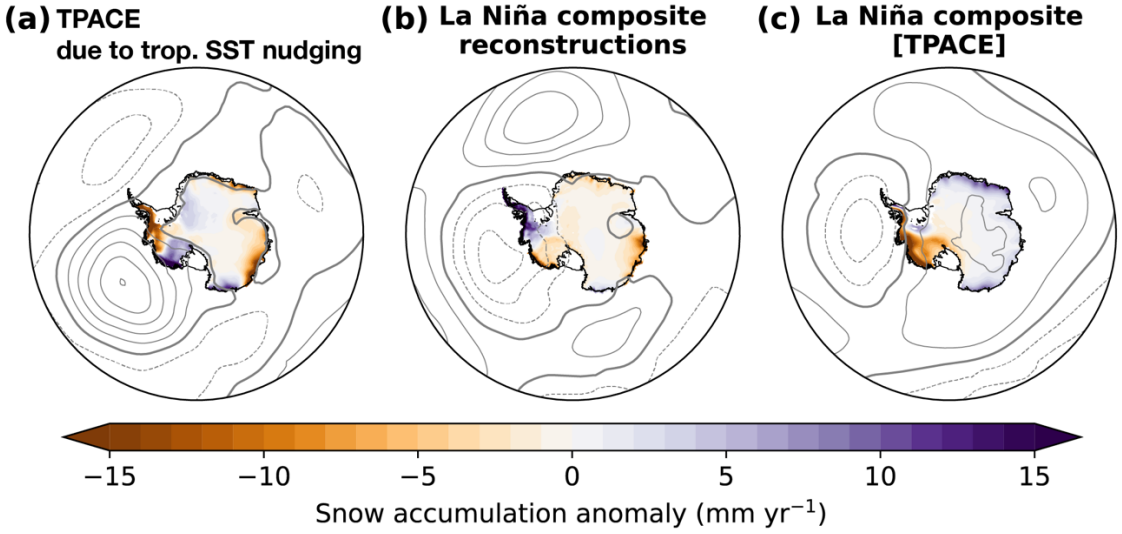

Figure C5. (a) Tropically driven ([TPACE] - [CESM2-LE*]) trend patterns in SLP and snow accumulation (1976:2000 minus 1901:1925). (b, c) Composites of snow accumulation and SLP anomalies during La Niña years over 1901-2000. Accumulation and SLP timeseries were linearly detrended before forming the composites. La Niña years are defined from NOAA's extended multivariate ENSO index, using austral autumn (MAM) values (https://psl.noaa.gov/enso/mei.ext/). The years composited are 1902, 1904, 1907, 1908, 1909, 1910, 1911, 1913, 1916, 1917, 1921, 1950, 1955, 1956, 1963, 1971, 1974, 1975, 1976, 1982, 1985, 1989, 1991, 1999, and 2000. SLP contours (gray lines) are in intervals of 0.25 hPa. Negative SLP values are dotted lines and positive values are solid lines; the zero contour is a heavier solid line.

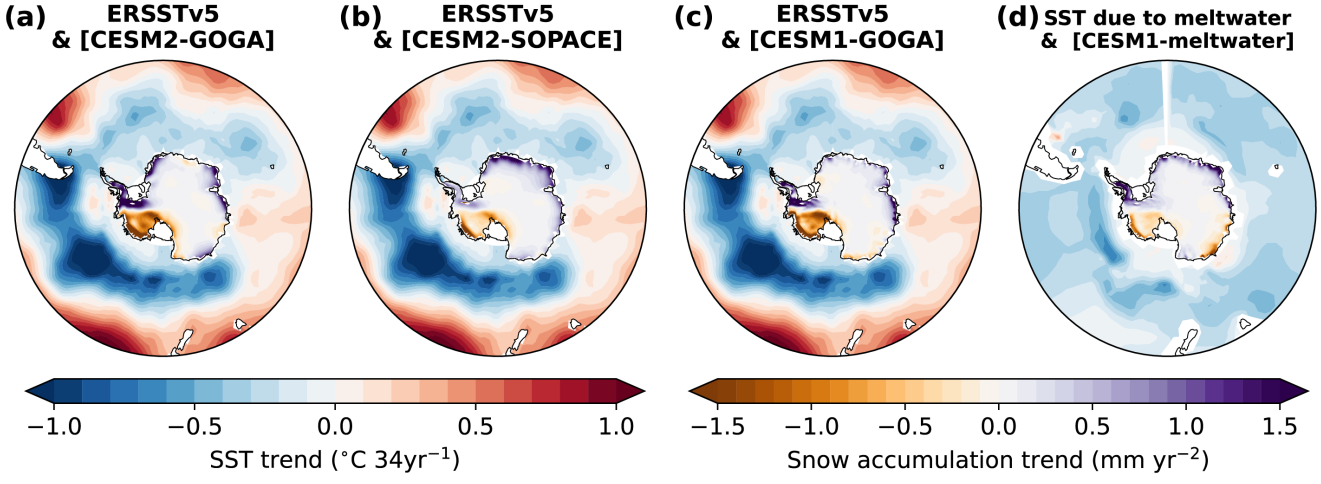

Figure C6. As in Fig. 8 but including results from the CESM Southern Ocean Pacemaker experiment that was nudged to SST anomalies from ERSSTv5 over the Southern Ocean (Kang et al., 2023). Data from CESM2 Southern Ocean Pacemaker provided by Yue Yu and Sarah Kang.

https://doi.org/10.5194/egusphere-2025-3666
Preprint. Discussion started: 16 September 2025

Appendix D. Trends in ERA5 since 1950

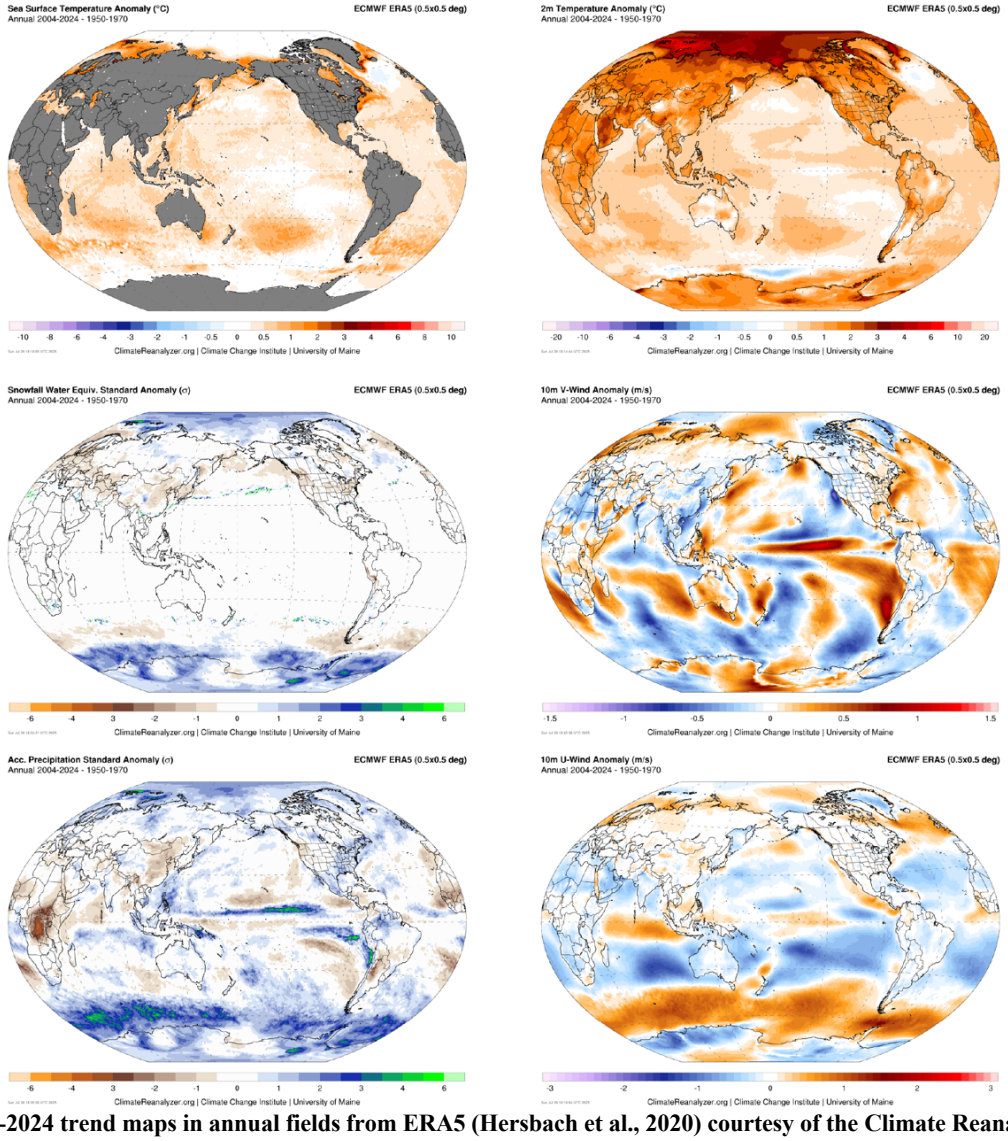

Figure D1. 1950-2024 trend maps in annual fields from ERA5 (Hersbach et al., 2020) courtesy of the Climate Reanalyzer (https://climatereanalyzer.org/research_tools/monthly_maps/). These maps support the trends and relationships inferred from paleoclimate data assimilation and CESM2 discussed in the main text, and the argument that these patterns have been in motion since the mid-twentieth century. Variables include SST, SAT, snowfall (standardized), 10-m meridional wind, accumulated precipitation (standardized) and 10-m zonal wind.

https://doi.org/10.5194/egusphere-2025-3666
Preprint. Discussion started: 16 September 2025

Code and data availability

Links to public archives of the data analyzed in this study are provided in the tables below. Code for creating the key figures has been deposited on Zenodo (Yin, 2025). An interactive visualizer of the PDA reconstructions with different model priors is available at https://jortuck.github.io/PaleoclimateVisualizer/.

Data availability and references for the CESM experiments analysed in this study.

abbreviation(s)	data access	main reference(s)
GHG, AAER, BMB, and EE	https://doi.org/10.26024/yw4w-1w27	Simpson et al. (2023)
CESM2-LE and CESM2-LEcmip6	https://doi.org/10.26024/KGMP-C556	Rodgers et al. (2021)
CESM2-TPACE	https://doi.org/10.26024/GTRS-TF57	Rosenbloom et al. (2022)
CESM2-GOGA and CESM2-TOGA	https://doi.org/10.26024/800d-nj44	Phillips and Simpson (2024)
CESM2-WNUDGE	https://doi.org/10.5281/zenodo.16459492	Espinosa et al. (2024)
CESM1-AIS meltwater	https://doi.org/10.5281/zenodo.7072847	Pauling et al. (2016); Dong et al. (2022a)
CESM2 piControl	https://doi.org/10.22033/ESGF/CMIP6.7733	Danabasoglu et al. (2019; 2020)
CESM1-GOGA	https://www.earthsystemgrid.org/dataset/ucar.cgd.ccsm4.cam5.prescribed_sst_amip.html	CESM Climate Variability and Change Working Group

Data availability and references for observational datasets, reconstructions and reanalysis products analysed in this study.

abbreviation(s)	data access	main reference(s)
MT19 snow accumulation	https://earth.gsfc.nasa.gov/cryo/data/antarctic-accumulation-reconstructions	Medley and Thomas (2019)
CESM1-LE PDA	https://doi.org/10.5281/zenodo.5507606	O'Connor et al. (2021)
CESM2-LE PDA	https://zenodo.org/records/15243743	O'Connor et al. (in press)
ERSSTv5	https://doi.org/10.7289/V5T72FNM	Huang et al. (2017)
ERA5	https://doi.org/10.24381/cds.f17050d7	Hersbach et al. (2020)
ERA20C	https://doi.org/10.5065/D6VQ30QG	Poli et al. (2016)

Author contributions

DPS conceptualized the overall study, obtained primary funding, curated datasets and led the writing of the paper. ZY was the primary contributor to the analysis code and figures, with contributions from DPS and GKO. GKO conceptualized, produced and verified the PDA reconstructions. EBW and ZE conceptualized and produced the wind-nudged experiment. ZIC and RTD contributed to analysis and

https://doi.org/10.5194/egusphere-2025-3666
Preprint. Discussion started: 16 September 2025

interpretation. DPS, ZY, EBW and RTD mentored students involved in the project. All authors discussed results and reviewed the manuscript.

Competing Interests

The authors declare that they have no conflict of interest.

Acknowledgements

The authors thank all the scientists, software engineers and administrators who contributed to the development of CESM, which is primarily supported by the US National Science Foundation (NSF). The CESM Climate Variability and Change Working Group led the production of the CESM2 Large Ensemble, and the CESM2 GOGA, TOGA, TPACE, and the single-forcing large ensembles. The authors acknowledge computing support on the Casper and Derecho systems (https://doi.org/10.5065/qx9a-pg09) provided by the NSF NCAR Computational and Information Systems Laboratory.

The authors thank Brooke Medley and Elizabeth Thomas for their snow accumulation reconstructions, and the innumerable scientists, technicians and support staff who contributed to collecting ice core, tree-ring and coral proxy data.

DPS appreciates Jan Lenaerts for collaboration in acquiring funding under NSF grant 1952199, and Jan Lenaerts and Devon Dunmire for guidance in working with snow accumulation data on the CESM grid. DPS thanks Yue Dong and Andrew Pauling for assistance with data from the CESM1 meltwater experiment. DPS thanks Yue Dong and Eric Steig for insightful discussions that helped improve this work.

Financial Support

DPS, ZY, ZIC, and RTD were supported by the US National Science Foundation (NSF) Office of Polar Programs (OPP) grant #1952199. DPS received additional support from the NSF NCAR, which is a major facility sponsored by the NSF, under cooperative agreement #1852977, and from a CIRES Innovative Research Program grant at University of Colorado Boulder. ZY received additional support from NSF HDR Institute, grant #2118285. GKO was supported by the Washington Research Foundation postdoctoral fellowship. EBW received support from NSF OPP grant #2213988. ZIC received additional support from the NSF-sponsored Significant Opportunities in Atmospheric Research and Science (SOARS) program.

https://doi.org/10.5194/egusphere-2025-3666
Preprint. Discussion started: 16 September 2025

ZE was supported by the U.S. Department of Energy, Office of Science, Office of Advanced Scientific Computing Research, Department of Energy Computational Science Graduate Fellowship under Award Number(s) DE-SC0023112. This report was prepared as an account of work sponsored by an agency of the United States Government. Neither the United States Government nor any agency thereof, nor any of their employees, makes any warranty, express or implied, or assumes any legal liability or responsibility for the accuracy, completeness, or usefulness of any information, apparatus, product, or process disclosed, or represents that its use would not infringe privately owned rights. Reference herein to any specific commercial product, process, or service by trade name, trademark, manufacturer, or otherwise does not necessarily constitute or imply its endorsement, recommendation, or favoring by the United States Government or any agency thereof. The views and opinions of authors expressed herein do not necessarily state or reflect those of the United States Government or any agency thereof.

References

Andrews, T., Bodas-Salcedo, A., Gregory, J. M., Dong, Y., Armour, K. C., Paynter, D., Lin, P., Modak, A., Mauritsen, T., Cole, J. N. S., Medeiros, B., Benedict, J. J., Douville, H., Roehrig, R., Koshiro, T., Kawai, H., Ogura, T., Dufresne, J., Allan, R. P., and Liu, C.: On the Effect of Historical SST Patterns on Radiative Feedback, JGR Atmospheres, 127, https://doi.org/10.1029/2022jd036675, 2022.

Armour, K. C., Proistosescu, C., Dong, Y., Hahn, L. C., Blanchard-Wrigglesworth, E., Pauling, A. G., Jnglin Wills, R. C., Andrews, T., Stuecker, M. F., Po-Chedley, S., Mitevski, I., Forster, P. M., and Gregory, J. M.: Sea-surface temperature pattern effects have slowed global warming and biased warming-based constraints on climate sensitivity, Proc. Natl. Acad. Sci. U.S.A., 121, https://doi.org/10.1073/pnas.2312093121, 2024.

Ashok, K. and Yamagata, T.: The El Niño with a difference, Nature, 461, 481–484, https://doi.org/10.1038/461481a, 2009.

Blanchard-Wrigglesworth, E., Roach, L. A., Donohoe, A., and Ding, Q.: Impact of Winds and Southern Ocean SSTs on Antarctic Sea Ice Trends and Variability, Journal of Climate, 34, 949–965, https://doi.org/10.1175/jcli-d-20-0386.1, 2021.

Blanchard-Wrigglesworth, E., Cox, T., Espinosa, Z. I., and Donohoe, A.: The Largest Ever Recorded Heatwave—Characteristics and Attribution of the Antarctic Heatwave of March 2022, Geophysical Research Letters, 50, https://doi.org/10.1029/2023gl104910, 2023.

https://doi.org/10.5194/egusphere-2025-3666
Preprint. Discussion started: 16 September 2025

Casado, M., Hébert, R., Faranda, D., and Landais, A.: The quandary of detecting the signature of climate change in Antarctica, Nat. Clim. Chang., 13, 1082–1088, https://doi.org/10.1038/s41558-023-01791-5, 2023.

Chang, P., Zhang, S., Danabasoglu, G., Yeager, S. G., Fu, H., Wang, H., Castruccio, F. S., Chen, Y., Edwards, J., Fu, D., Jia, Y., Laurindo, L. C., Liu, X., Rosenbloom, N., Small, R. J., Xu, G., Zeng, Y., Zhang, Q., Bacmeister, J., Bailey, D. A., Duan, X., DuVivier, A. K., Li, D., Li, Y., Neale, R., Stössel, A., Wang, L., Zhuang, Y., Baker, A., Bates, S., Dennis, J., Diao, X., Gan, B., Gopal, A., Jia, D., Jing, Z., Ma, X., Saravanan, R., Strand, W. G., Tao, J., Yang, H., Wang, X., Wei, Z., and Wu, L.: An Unprecedented Set of High-Resolution Earth System Simulations for Understanding Multiscale Interactions in Climate Variability and Change, J Adv Model Earth Syst, 12, https://doi.org/10.1029/2020ms002298, 2020.

Chemke, R., Previdi, M., England, M. R., and Polvani, L. M.: Distinguishing the impacts of ozone and ozone-depleting substances on the recent increase in Antarctic surface mass balance, The Cryosphere, 14, 4135–4144, https://doi.org/10.5194/tc-14-4135-2020, 2020.

Chung, E.-S., Kim, S.-J., Timmermann, A., Ha, K.-J., Lee, S.-K., Stuecker, M. F., Rodgers, K. B., Lee, S.-S., and Huang, L.: Antarctic sea-ice expansion and Southern Ocean cooling linked to tropical variability, Nat. Clim. Chang., 12, 461–468, https://doi.org/10.1038/s41558-022-01339-z, 2022.

Clark, R. W., Wellner, J. S., Hillenbrand, C.-D., Totten, R. L., Smith, J. A., Miller, L. E., Larter, R. D., Hogan, K. A., Graham, A. G. C., Nitsche, F. O., Lehrmann, A. A., Lepp, A. P., Kirkham, J. D., Fitzgerald, V. T., Garcia-Barrera, G., Ehrmann, W., and Wacker, L.: Synchronous retreat of Thwaites and Pine Island glaciers in response to external forcings in the presatellite era, Proc. Natl. Acad. Sci. U.S.A., 121, https://doi.org/10.1073/pnas.2211711120, 2024.

Clem, K. R., Adusumilli, S., Baiman, R., Banwell, A. F., Barreira, S., Beadling, R. L., Bozkurt, D., Colwell, S., Coy, L., Datta, R. T., De Laat, J., du Plessis, M., Dunmire, D., Fogt, R. L., Freeman, N. M., Fricker, H. A., Gardner, A. S., Gille, S. T., Johnson, B., Josey, S. A., Keller, L. M., Kramarova, N. A., Lazzara, M. A., Lieser, J. L., MacFerrin, M., MacGilchrist, G. A., MacLennan, M. L., Massom, R. A., Mazloff, M. R., Mikolajczyk, D. E., Mote, T. L., Nash, E. R., Newman, P. A., Norton, T., Ochwat, N., Petropavlovskikh, I., Pezzi, L. P., Pitts, M., Raphael, M. N., Reid, P., Santee, M. L., Santini, M., Scambos, T., Schultz, C., Shi, J.-R., Souza, E., Stammerjohn, S., Strahan, S. E., Thompson, A. F., Trusel, L. D., Wille, J. D., Yin, Z., Allen, J., Camper, A. V., Haley, B. O., Hammer, G., Love-Brotak, S. E., Ohlmann, L., Noguchi, L., Riddle, D. B., and Veasey, S. W.: Antarctica and the Southern Ocean, Bulletin of the American Meteorological Society, 104, S322–S365, https://doi.org/10.1175/bams-d-23-0077.1, 2023.

Climate Reanalyzer: Monthly Reanalysis Maps. Climate Change Institute, University of Maine. Retrieved 20 July 2025, from https://climatereanalyzer.org/

https://doi.org/10.5194/egusphere-2025-3666
Preprint. Discussion started: 16 September 2025

Copernicus Climate Change Service: ERA5 monthly averaged data on single levels from 1940 to present, https://doi.org/10.24381/CDS.F17050D7, 2019.

Dalaiden, Q., Abram, N. J., Goosse, H., Holland, P. R., O'Connor, G. K., and Topál, D.: Multi-Decadal Variability of Amundsen Sea Low Controlled by Natural Tropical and Anthropogenic Drivers, Geophysical Research Letters, 51, https://doi.org/10.1029/2024gl109137, 2024.

Dalaiden, Q., Goosse, H., Klein, F., Lenaerts, J. T. M., Holloway, M., Sime, L., and Thomas, E. R.: How useful is snow accumulation in reconstructing surface air temperature in Antarctica? A study combining ice core records and climate models, The Cryosphere, 14, 1187–1207, https://doi.org/10.5194/tc-14-1187-2020, 2020.

Dalaiden, Q., Schurer, A. P., Kirchmeier-Young, M. C., Goosse, H., and Hegerl, G. C.: West Antarctic Surface Climate Changes Since the Mid-20th Century Driven by Anthropogenic Forcing, Geophysical Research Letters, 49, https://doi.org/10.1029/2022gl099543, 2022.

Danabasoglu, G., Lawrence, D., Lindsay, K., Lipscomb, W., and Strand, G.: NCAR CESM2 model output prepared for CMIP6 CMIP piControl (20250528), https://doi.org/10.22033/ESGF/CMIP6.7733, 2019.

Danabasoglu, G., Lamarque, J. -F., Bacmeister, J., Bailey, D. A., DuVivier, A. K., Edwards, J., Emmons, L. K., Fasullo, J., Garcia, R., Gettelman, A., Hannay, C., Holland, M. M., Large, W. G., Lauritzen, P. H., Lawrence, D. M., Lenaerts, J. T. M., Lindsay, K., Lipscomb, W. H., Mills, M. J., Neale, R., Oleson, K. W., Otto-Bliesner, B., Phillips, A. S., Sacks, W., Tilmes, S., van Kampenhout, L., Vertenstein, M., Bertini, A., Dennis, J., Deser, C., Fischer, C., Fox-Kemper, B., Kay, J. E., Kinnison, D., Kushner, P. J., Larson, V. E., Long, M. C., Mickelson, S., Moore, J. K., Nienhouse, E., Polvani, L., Rasch, P. J., and Strand, W. G.: The Community Earth System Model Version 2 (CESM2), J Adv Model Earth Syst, 12, https://doi.org/10.1029/2019ms001916, 2020.

Datta, R. T., Herrington, A., Lenaerts, J. T. M., Schneider, D. P., Trusel, L., Yin, Z., and Dunmire, D.: Evaluating the impact of enhanced horizontal resolution over the Antarctic domain using a variable-resolution Earth system model, The Cryosphere, 17, 3847–3866, https://doi.org/10.5194/tc-17-3847-2023, 2023.

Dong, Y.: Data for "Antarctic ice-sheet meltwater reduces transient warming and climate sensitivity through the sea-surface temperature pattern effect," https://doi.org/10.5281/ZENODO.7072847, 2022.

Dong, Y., Pauling, A. G., Sadai, S., and Armour, K. C.: Antarctic Ice-Sheet Meltwater Reduces Transient Warming and Climate Sensitivity Through the Sea-Surface Temperature Pattern Effect, Geophysical Research Letters, 49, https://doi.org/10.1029/2022gl101249, 2022a.

https://doi.org/10.5194/egusphere-2025-3666
Preprint. Discussion started: 16 September 2025

Dong, Y., Armour, K. C., Battisti, D. S., and Blanchard-Wrigglesworth, E.: Two-Way Teleconnections between the Southern Ocean and the Tropical Pacific via a Dynamic Feedback, Journal of Climate, 35, 6267–6282, https://doi.org/10.1175/jcli-d-22-0080.1, 2022b.

Dong, Y., Polvani, L. M., Hwang, Y.-T., and England, M. R.: Stratospheric ozone depletion has contributed to the recent tropical La Niña-like cooling pattern, npj Clim Atmos Sci, 8, https://doi.org/10.1038/s41612-025-01020-0, 2025.

Dunmire, D., Lenaerts, J. T. M., Datta, R. T., and Gorte, T.: Antarctic surface climate and surface mass balance in the Community Earth System Model version 2 during the satellite era and into the future (1979–2100), The Cryosphere, 16, 4163–4184, https://doi.org/10.5194/tc-16-4163-2022, 2022.

Espinosa, Z.: Wind-Nudging Data for Schneider et. al. 2025: Antarctic Snow Fall (0.1), https://doi.org/10.5281/ZENODO.16459492, 2025.

Espinosa, Z. I., Blanchard-Wrigglesworth, E., and Bitz, C. M.: Understanding the drivers and predictability of record low Antarctic sea ice in austral winter 2023, Commun Earth Environ, 5, https://doi.org/10.1038/s43247-024-01772-2, 2024.

Eswaran, A., Truax, O. J., and Fudge, T. J.: 20th-Century Antarctic Sea Level Mitigation Driven by Uncertain East Antarctic Accumulation History, Geophysical Research Letters, 51, https://doi.org/10.1029/2023gl106991, 2024.

European Centre For Medium-Range Weather Forecasts: ERA-20C Project (ECMWF Atmospheric Reanalysis of the 20th Century), https://doi.org/10.5065/D6VQ30QG, 2014.

Fan, T., Deser, C., and Schneider, D. P.: Recent Antarctic sea ice trends in the context of Southern Ocean surface climate variations since 1950, Geophys. Res. Lett., 41, 2419–2426, https://doi.org/10.1002/2014gl059239, 2014.

Fasullo, J. T., Lamarque, J., Hannay, C., Rosenbloom, N., Tilmes, S., DeRepentigny, P., Jahn, A., and Deser, C.: Spurious Late Historical-Era Warming in CESM2 Driven by Prescribed Biomass Burning Emissions, Geophysical Research Letters, 49, https://doi.org/10.1029/2021gl097420, 2022.

Fox-Kemper, B et al.: Ocean, Cryosphere and Sea Level Change, Climate Change 2021 – The Physical Science Basis, 1211–1362, https://doi.org/10.1017/9781009157896.011, 2023.

Frieler, K., Clark, P. U., He, F., Buizert, C., Reese, R., Ligtenberg, S. R. M., van den Broeke, M. R., Winkelmann, R., and Levermann, A.: Consistent evidence of increasing Antarctic accumulation with warming, Nature Clim Change, 5, 348–352, https://doi.org/10.1038/nclimate2574, 2015.

https://doi.org/10.5194/egusphere-2025-3666
Preprint. Discussion started: 16 September 2025

Gelaro, R., McCarty, W., Suárez, M. J., Todling, R., Molod, A., Takacs, L., Randles, C. A., Darmenov, A., Bosilovich, M. G., Reichle, R., Wargan, K., Coy, L., Cullather, R., Draper, C., Akella, S., Buchard, V., Conaty, A., da Silva, A. M., Gu, W., Kim, G.-K., Koster, R., Lucchesi, R., Merkova, D., Nielsen, J. E., Partyka, G., Pawson, S., Putman, W., Rienecker, M., Schubert, S. D., Sienkiewicz, M., and Zhao, B.: The Modern-Era Retrospective Analysis for Research and Applications, Version 2 (MERRA-2), J. Climate, 30, 5419–5454, https://doi.org/10.1175/jcli-d-16-0758.1, 2017.

Genthon, C., Krinner, G., and Sacchettini, M.: Interannual Antarctic tropospheric circulation and precipitation variability, Climate Dynamics, 21, 289–307, https://doi.org/10.1007/s00382-003-0329-1, 2003.

Gettelman, A., Hannay, C., Bacmeister, J. T., Neale, R. B., Pendergrass, A. G., Danabasoglu, G., Lamarque, J. -F., Fasullo, J. T., Bailey, D. A., Lawrence, D. M., and Mills, M. J.: High Climate Sensitivity in the Community Earth System Model Version 2 (CESM2), Geophysical Research Letters, 46, 8329–8337, https://doi.org/10.1029/2019gl083978, 2019.

Gettelman, A., Mills, M. J., Kinnison, D. E., Garcia, R. R., Smith, A. K., Marsh, D. R., Tilmes, S., Vitt, F., Bardeen, C. G., McInerny, J., Liu, H. -L., Solomon, S. C., Polvani, L. M., Emmons, L. K., Lamarque, J. -F., Richter, J. H., Glanville, A. S., Bacmeister, J. T., Phillips, A. S., Neale, R. B., Simpson, I. R., DuVivier, A. K., Hodzic, A., and Randel, W. J.: The Whole Atmosphere Community Climate Model Version 6 (WACCM6), JGR Atmospheres, 124, 12380–12403, https://doi.org/10.1029/2019jd030943, 2019.

Gilbert, E. and Kittel, C.: Surface Melt and Runoff on Antarctic Ice Shelves at 1.5°C, 2°C, and 4°C of Future Warming, Geophysical Research Letters, 48, https://doi.org/10.1029/2020gl091733, 2021.

Hartmann, D. L.: The Antarctic ozone hole and the pattern effect on climate sensitivity, Proc. Natl. Acad. Sci. U.S.A., 119, https://doi.org/10.1073/pnas.2207889119, 2022.

Heede, U. K. and Fedorov, A. V.: Eastern equatorial Pacific warming delayed by aerosols and thermostat response to CO2 increase, Nat. Clim. Chang., 11, 696–703, https://doi.org/10.1038/s41558-021-01101-x, 2021.

Henley, B. J., Gergis, J., Karoly, D. J., Power, S., Kennedy, J., and Folland, C. K.: A Tripole Index for the Interdecadal Pacific Oscillation, Clim Dyn, 45, 3077–3090, https://doi.org/10.1007/s00382-015-2525-1, 2015.

Hersbach, H., Bell, B., Berrisford, P., Hirahara, S., Horányi, A., Muñoz-Sabater, J., Nicolas, J., Peubey, C., Radu, R., Schepers, D., Simmons, A., Soci, C., Abdalla, S., Abellan, X., Balsamo, G., Bechtold, P., Biavati, G., Bidlot, J., Bonavita, M., De Chiara, G., Dahlgren, P., Dee, D., Diamantakis, M., Dragani, R., Flemming, J., Forbes, R., Fuentes, M., Geer, A., Haimberger, L., Healy, S., Hogan, R. J., Hólm, E., Janisková, M., Keeley, S., Laloyaux, P., Lopez, P., Lupu, C., Radnoti, G., de Rosnay, P., Rozum, I.,

https://doi.org/10.5194/egusphere-2025-3666
Preprint. Discussion started: 16 September 2025

Vamborg, F., Villaume, S., and Thépaut, J.: The ERA5 global reanalysis, Quart J Royal Meteoro Soc, 146, 1999–2049, https://doi.org/10.1002/qj.3803, 2020.

Holland, P. R., O'Connor, G. K., Bracegirdle, T. J., Dutrieux, P., Naughten, K. A., Steig, E. J., Schneider, D. P., Jenkins, A., and Smith, J. A.: Anthropogenic and internal drivers of wind changes over the Amundsen Sea, West Antarctica, during the 20th and 21st centuries, The Cryosphere, 16, 5085–5105, https://doi.org/10.5194/tc-16-5085-2022, 2022.

Huang, B., Thorne, P. W., Banzon, V. F., Boyer, T., Chepurin, G., Lawrimore, J. H., Menne, M. J., Smith, T. M., Vose, R. S., and Zhang, H.-M.: NOAA Extended Reconstructed Sea Surface Temperature (ERSST), Version 5, https://doi.org/10.7289/V5T72FNM, 2017.

Huang, B., Thorne, P. W., Banzon, V. F., Boyer, T., Chepurin, G., Lawrimore, J. H., Menne, M. J., Smith, T. M., Vose, R. S., and Zhang, H.-M.: Extended Reconstructed Sea Surface Temperature, Version 5 (ERSSTv5): Upgrades, Validations, and Intercomparisons, Journal of Climate, 30, 8179–8205, https://doi.org/10.1175/jcli-d-16-0836.1, 2017.

Hurrell, J. W., Holland, M. M., Gent, P. R., Ghan, S., Kay, J. E., Kushner, P. J., Lamarque, J.-F., Large, W. G., Lawrence, D., Lindsay, K., Lipscomb, W. H., Long, M. C., Mahowald, N., Marsh, D. R., Neale, R. B., Rasch, P., Vavrus, S., Vertenstein, M., Bader, D., Collins, W. D., Hack, J. J., Kiehl, J., and Marshall, S.: The Community Earth System Model: A Framework for Collaborative Research, Bull. Amer. Meteor. Soc., 94, 1339–1360, https://doi.org/10.1175/bams-d-12-00121.1, 2013.

IBS Center for Climate Physics, National Center for Atmospheric Research, Danabasoglu, G., Deser, C., Rodgers, K., and Timmermann, A.: CESM2 Large Ensemble Community Project, https://doi.org/10.26024/KGMP-C556, 2021.

Jones, M. E., Bromwich, D. H., Nicolas, J. P., Carrasco, J., Plavcová, E., Zou, X., and Wang, S.-H.: Sixty Years of Widespread Warming in the Southern Middle and High Latitudes (1957–2016), Journal of Climate, 32, 6875–6898, https://doi.org/10.1175/jcli-d-18-0565.1, 2019.

Kang, S. M., Yu, Y., Deser, C., Zhang, X., Kang, I.-S., Lee, S.-S., Rodgers, K. B., and Ceppi, P.: Global impacts of recent Southern Ocean cooling, Proc. Natl. Acad. Sci. U.S.A., 120, https://doi.org/10.1073/pnas.2300881120, 2023.

Kay, J. E., Deser, C., Phillips, A., Mai, A., Hannay, C., Strand, G., Arblaster, J. M., Bates, S. C., Danabasoglu, G., Edwards, J., Holland, M., Kushner, P., Lamarque, J.-F., Lawrence, D., Lindsay, K., Middleton, A., Munoz, E., Neale, R., Oleson, K., Polvani, L., and Vertenstein, M.: The Community Earth System Model (CESM) Large Ensemble Project: A Community Resource for Studying Climate Change in the Presence of Internal Climate Variability, Bulletin of the American Meteorological Society, 96, 1333–1349, https://doi.org/10.1175/bams-d-13-00255.1, 2015.

https://doi.org/10.5194/egusphere-2025-3666
Preprint. Discussion started: 16 September 2025

Kim, H., Kang, S. M., Kay, J. E., and Xie, S.-P.: Subtropical clouds key to Southern Ocean teleconnections to the tropical Pacific, Proc. Natl. Acad. Sci. U.S.A., 119, https://doi.org/10.1073/pnas.2200514119, 2022.

King, M. A. and Christoffersen, P.: Major Modes of Climate Variability Dominate Nonlinear Antarctic Ice-Sheet Elevation Changes 2002–2020, Geophysical Research Letters, 51, https://doi.org/10.1029/2024gl108844, 2024.

Lee, S., L'Heureux, M., Wittenberg, A. T., Seager, R., O'Gorman, P. A., and Johnson, N. C.: On the future zonal contrasts of equatorial Pacific climate: Perspectives from Observations, Simulations, and Theories, npj Clim Atmos Sci, 5, https://doi.org/10.1038/s41612-022-00301-2, 2022.

Lenaerts, J. T. M., Fyke, J., and Medley, B.: The Signature of Ozone Depletion in Recent Antarctic Precipitation Change: A Study With the Community Earth System Model, Geophysical Research Letters, 45, https://doi.org/10.1029/2018gl078608, 2018.

Lenaerts, J. T. M., Medley, B., van den Broeke, M. R., and Wouters, B.: Observing and Modeling Ice Sheet Surface Mass Balance, Reviews of Geophysics, 57, 376–420, https://doi.org/10.1029/2018rg000622, 2019.

Lenssen, N. J. L., Schmidt, G. A., Hansen, J. E., Menne, M. J., Persin, A., Ruedy, R., and Zyss, D.: Improvements in the GISTEMP Uncertainty Model, JGR Atmospheres, 124, 6307–6326, https://doi.org/10.1029/2018jd029522, 2019.

Li, X., Cai, W., Meehl, G. A., Chen, D., Yuan, X., Raphael, M., Holland, D. M., Ding, Q., Fogt, R. L., Markle, B. R., Wang, G., Bromwich, D. H., Turner, J., Xie, S.-P., Steig, E. J., Gille, S. T., Xiao, C., Wu, B., Lazzara, M. A., Chen, X., Stammerjohn, S., Holland, P. R., Holland, M. M., Cheng, X., Price, S. F., Wang, Z., Bitz, C. M., Shi, J., Gerber, E. P., Liang, X., Goosse, H., Yoo, C., Ding, M., Geng, L., Xin, M., Li, C., Dou, T., Liu, C., Sun, W., Wang, X., and Song, C.: Tropical teleconnection impacts on Antarctic climate changes, Nat Rev Earth Environ, 2, 680–698, https://doi.org/10.1038/s43017-021-00204-5, 2021.

Marshall, G. J.: Trends in the Southern Annular Mode from Observations and Reanalyses, J. Climate, 16, 4134–4143, https://doi.org/10.1175/1520-0442(2003)016<4134:titsam>2.0.co;2, 2003.

Medley, B., McConnell, J. R., Neumann, T. A., Reijmer, C. H., Chellman, N., Sigl, M., and Kipfstuhl, S.: Temperature and Snowfall in Western Queen Maud Land Increasing Faster Than Climate Model Projections, Geophysical Research Letters, 45, 1472–1480, https://doi.org/10.1002/2017gl075992, 2018.

https://doi.org/10.5194/egusphere-2025-3666
Preprint. Discussion started: 16 September 2025

Medley, B. and Thomas, E. R.: Increased snowfall over the Antarctic Ice Sheet mitigated twentieth-century sea-level rise, Nature Clim Change, 9, 34–39, https://doi.org/10.1038/s41558-018-0356-x, 2019.

Monaghan, A. J., Bromwich, D. H., Fogt, R. L., Wang, S.-H., Mayewski, P. A., Dixon, D. A., Ekaykin, A., Frezzotti, M., Goodwin, I., Isaksson, E., Kaspari, S. D., Morgan, V. I., Oerter, H., Van Ommen, T. D., Van der Veen, C. J., and Wen, J.: Insignificant Change in Antarctic Snowfall Since the International Geophysical Year, Science, 313, 827–831, https://doi.org/10.1126/science.1128243, 2006.

Monaghan, A. J., Bromwich, D. H., and Schneider, D. P.: Twentieth century Antarctic air temperature and snowfall simulations by IPCC climate models, Geophysical Research Letters, 35, https://doi.org/10.1029/2007gl032630, 2008.

Morice, C. P., Kennedy, J. J., Rayner, N. A., Winn, J. P., Hogan, E., Killick, R. E., Dunn, R. J. H., Osborn, T. J., Jones, P. D., and Simpson, I. R.: An Updated Assessment of Near-Surface Temperature Change From 1850: The HadCRUT5 Data Set, JGR Atmospheres, 126, https://doi.org/10.1029/2019jd032361, 2021.

Mottram, R., Hansen, N., Kittel, C., van Wessem, J. M., Agosta, C., Amory, C., Boberg, F., van de Berg, W. J., Fettweis, X., Gossart, A., van Lipzig, N. P. M., van Meijgaard, E., Orr, A., Phillips, T., Webster, S., Simonsen, S. B., and Souverijns, N.: What is the surface mass balance of Antarctica? An intercomparison of regional climate model estimates, The Cryosphere, 15, 3751–3784, https://doi.org/10.5194/tc-15-3751-2021, 2021.

Mottram, R., van den Broeke, M., Meijers, A., Rodehacke, C., Dell, R. L., Hogg, A. E., Davison, B. J., Lhermitte, S., Hansen, N., Torres Alavez, J. A., and Olesen, M.: Determining the Freshwater Fluxes from Antarctica with Earth Observation Data, Models, and In Situ Measurements: Uncertainties, Knowledge Gaps, and Prospects for New Advances, Bulletin of the American Meteorological Society, 105, E1371–E1379, https://doi.org/10.1175/bams-d-24-0002.1, 2024.

Naakka, T., Nygård, T., and Vihma, T.: Air Moisture Climatology and Related Physical Processes in the Antarctic on the Basis of ERA5 Reanalysis, Journal of Climate, 34, 4463–4480, https://doi.org/10.1175/jcli-d-20-0798.1, 2021.

Neff, P.: Amundsen Sea Coastal Ice Rises: Future Sites for Marine-Focused Ice Core Records, Oceanog, 33, https://doi.org/10.5670/oceanog.2020.215, 2020.

Nicola, L., Notz, D., and Winkelmann, R.: Revisiting temperature sensitivity: how does Antarctic precipitation change with temperature?, The Cryosphere, 17, 2563–2583, https://doi.org/10.5194/tc-17-2563-2023, 2023.

https://doi.org/10.5194/egusphere-2025-3666
Preprint. Discussion started: 16 September 2025

Noël, B., van Wessem, J. M., Wouters, B., Trusel, L., Lhermitte, S., and van den Broeke, M. R.: Higher Antarctic ice sheet accumulation and surface melt rates revealed at 2 km resolution, Nat Commun, 14, https://doi.org/10.1038/s41467-023-43584-6, 2023.

O'Connor, G. K., Steig, E. J., and Hakim, G. J.: Strengthening Southern Hemisphere Westerlies and Amundsen Sea Low Deepening Over the 20th Century Revealed by Proxy-Data Assimilation, Geophysical Research Letters, 48, https://doi.org/10.1029/2021gl095999, 2021.

O'Connor, G. K., Steig, E. J., and Hakim, G. J.: Southern Hemisphere winds, pressure, and temperature over the 20th century from proxy-data assimilation, https://doi.org/10.5281/zenodo.5507606, 2021.

O'Connor, G.K., Nakayama, Y., Steig, E.J., Armour, K.C., Thompson, L., Hyogo, S., Berdahl, M., Shimada, T. Enhanced West Antarctic ice loss triggered by polynya response to meridional winds. Nature Geoscience, in press.

O'Connor, G., Nakayama, Y., Steig, E., Armour, K., Thompson, L., Hyogo, S., Berdahl, M., & Shimada, T. Proxy Reconstructions and Amundsen Sea Simulations with Repeated Atmospheric Forcings [Data set]. Zenodo. https://doi.org/10.5281/zenodo.15243743, 2025.

Palerme, C., Genthon, C., Claud, C., Kay, J. E., Wood, N. B., and L'Ecuyer, T.: Evaluation of current and projected Antarctic precipitation in CMIP5 models, Clim Dyn, 48, 225–239, https://doi.org/10.1007/s00382-016-3071-1, 2016.

Pauling, A. G., Bitz, C. M., Smith, I. J., and Langhorne, P. J.: The Response of the Southern Ocean and Antarctic Sea Ice to Freshwater from Ice Shelves in an Earth System Model, Journal of Climate, 29, 1655–1672, https://doi.org/10.1175/jcli-d-15-0501.1, 2016.

Phillips, A. and Simpson, I.: CAM6 Prescribed SST AMIP Ensembles, https://doi.org/10.26024/800D-NJ44, 2024.

Poli, P., Hersbach, H., Dee, D. P., Berrisford, P., Simmons, A. J., Vitart, F., Laloyaux, P., Tan, D. G. H., Peubey, C., Thépaut, J.-N., Trémolet, Y., Hólm, E. V., Bonavita, M., Isaksen, L., and Fisher, M.: ERA-20C: An Atmospheric Reanalysis of the Twentieth Century, Journal of Climate, 29, 4083–4097, https://doi.org/10.1175/jcli-d-15-0556.1, 2016.

Previdi, M. and Polvani, L. M.: Anthropogenic impact on Antarctic surface mass balance, currently masked by natural variability, to emerge by mid-century, Environ. Res. Lett., 11, 094001, https://doi.org/10.1088/1748-9326/11/9/094001, 2016.

Rignot, E., Mouginot, J., Scheuchl, B., van den Broeke, M., van Wessem, M. J., and Morlighem, M.: Four decades of Antarctic Ice Sheet mass balance from 1979–2017, Proc. Natl. Acad. Sci. U.S.A., 116, 1095–1103, https://doi.org/10.1073/pnas.1812883116, 2019.

Roach, L. A., Mankoff, K. D., Romanou, A., Blanchard-Wrigglesworth, E., Haine, T. W. N., and Schmidt, Gavin. A.: Winds and Meltwater Together Lead to Southern Ocean Surface Cooling and Sea Ice Expansion, Geophysical Research Letters, 50, https://doi.org/10.1029/2023gl105948, 2023.

Rodgers, K. B., Lee, S.-S., Rosenbloom, N., Timmermann, A., Danabasoglu, G., Deser, C., Edwards, J., Kim, J.-E., Simpson, I. R., Stein, K., Stuecker, M. F., Yamaguchi, R., Bódai, T., Chung, E.-S., Huang, L., Kim, W. M., Lamarque, J.-F., Lombardozzi, D. L., Wieder, W. R., and Yeager, S. G.: Ubiquity of human-induced changes in climate variability, Earth Syst. Dynam., 12, 1393–1411, https://doi.org/10.5194/esd-12-1393-2021, 2021.

Rosenbloom, Nan: CESM2 Pacific Pacemaker Ensemble, https://doi.org/10.26024/GTRS-TF57, 2022.

Rosier, S. H. R., Gudmundsson, G. H., Jenkins, A., and Naughten, K. A.: Calibrated sea level contribution from the Amundsen Sea sector, West Antarctica, under RCP8.5 and Paris 2C scenarios, The Cryosphere, 19, 2527–2557, https://doi.org/10.5194/tc-19-2527-2025, 2025.

Rye, C. D., Marshall, J., Kelley, M., Russell, G., Nazarenko, L. S., Kostov, Y., Schmidt, G. A., and Hansen, J.: Antarctic Glacial Melt as a Driver of Recent Southern Ocean Climate Trends, Geophysical Research Letters, 47, https://doi.org/10.1029/2019gl086892, 2020.

Sadai, S., Condron, A., DeConto, R., and Pollard, D.: Future climate response to Antarctic Ice Sheet melt caused by anthropogenic warming, Sci. Adv., 6, https://doi.org/10.1126/sciadv.aaz1169, 2020.

Schmidt, Gavin. A., Romanou, A., Roach, L. A., Mankoff, K. D., Li, Q., Rye, C. D., Kelley, M., Marshall, J. C., and Busecke, J. J. M.: Anomalous Meltwater From Ice Sheets and Ice Shelves Is a Historical Forcing, Geophysical Research Letters, 50, https://doi.org/10.1029/2023gl106530, 2023.

Schmidt, G. A., Mankoff, K. D., Bamber, J. L., Carroll, D., Chandler, D. M., Coulon, V., Davison, B. J., England, M. H., Holland, P. R., Jourdain, N. C., Li, Q., Marson, J. M., Mathiot, P., McMahon, C. R., Moon, T. A., Mottram, R., Nowicki, S., Olivé Abelló, A., Pauling, A. G., Rackow, T., and Ringeisen, D.: Datasets and protocols for including anomalous freshwater from melting ice sheets in climate simulations, , https://doi.org/10.5194/egusphere-2025-1940, 2025 (preprint).

Schneider, D. P. and Deser, C.: Tropically driven and externally forced patterns of Antarctic sea ice change: reconciling observed and modeled trends, Clim Dyn, 50, 4599–4618, https://doi.org/10.1007/s00382-017-3893-5, 2017.

Schneider, D. P., Kay, J. E., and Lenaerts, J.: Improved clouds over Southern Ocean amplify Antarctic precipitation response to ozone depletion in an earth system model, Clim Dyn, 55, 1665–1684, https://doi.org/10.1007/s00382-020-05346-8, 2020.

https://doi.org/10.5194/egusphere-2025-3666
Preprint. Discussion started: 16 September 2025

Schneider, D. P., Kay, J. E., and Hannay, C.: Cloud and Surface Albedo Feedbacks Reshape 21st Century Warming in Successive Generations of An Earth System Model, Geophysical Research Letters, 49, https://doi.org/10.1029/2022gl100653, 2022.

Schneider, D. P., Okumura, Y., and Deser, C.: Observed Antarctic Interannual Climate Variability and Tropical Linkages, Journal of Climate, 25, 4048–4066, https://doi.org/10.1175/jcli-d-11-00273.1, 2012.

Schneider, D. P. and Steig, E. J.: Ice cores record significant 1940s Antarctic warmth related to tropical climate variability, Proc. Natl. Acad. Sci. U.S.A., 105, 12154–12158, https://doi.org/10.1073/pnas.0803627105, 2008.

Shepherd, A., Gilbert, L., Muir, A. S., Konrad, H., McMillan, M., Slater, T., Briggs, K. H., Sundal, A. V., Hogg, A. E., and Engdahl, M. E.: Trends in Antarctic Ice Sheet Elevation and Mass, Geophysical Research Letters, 46, 8174–8183, https://doi.org/10.1029/2019gl082182, 2019.

Simpson, I. and Rosenbloom, N.: CESM2 Single Forcing Large Ensemble Project, https://doi.org/10.26024/YW4W-1W27, 2022.

Simpson, I. R., Rosenbloom, N., Danabasoglu, G., Deser, C., Yeager, S. G., McCluskey, C. S., Yamaguchi, R., Lamarque, J.-F., Tilmes, S., Mills, M. J., and Rodgers, K. B.: The CESM2 Single-Forcing Large Ensemble and Comparison to CESM1: Implications for Experimental Design, Journal of Climate, 36, 5687–5711, https://doi.org/10.1175/jcli-d-22-0666.1, 2023.

Simpson, I. R., Shaw, T. A., Ceppi, P., Clement, A. C., Fischer, E., Grise, K. M., Pendergrass, A. G., Screen, J. A., Wills, R. C. J., Woollings, T., Blackport, R., Kang, J. M., and Po-Chedley, S.: Confronting Earth System Model trends with observations, Sci. Adv., 11, https://doi.org/10.1126/sciadv.adt8035, 2025.

Smith, J. A., Andersen, T. J., Shortt, M., Gaffney, A. M., Truffer, M., Stanton, T. P., Bindschadler, R., Dutrieux, P., Jenkins, A., Hillenbrand, C.-D., Ehrmann, W., Corr, H. F. J., Farley, N., Crowhurst, S., and Vaughan, D. G.: Sub-ice-shelf sediments record history of twentieth-century retreat of Pine Island Glacier, Nature, 541, 77–80, https://doi.org/10.1038/nature20136, 2016.

Sodemann, H. and Stohl, A.: Asymmetries in the moisture origin of Antarctic precipitation, Geophysical Research Letters, 36, https://doi.org/10.1029/2009gl040242, 2009.

Stokes, C. R., Bamber, J. L., Dutton, A., and DeConto, R. M.: Warming of +1.5 °C is too high for polar ice sheets, Commun Earth Environ, 6, https://doi.org/10.1038/s43247-025-02299-w, 2025.

Swart, N., Martin, T., Beadling, R., Chen, J.-J., England, M. H., Farneti, R., Griffies, S. M., Hatterman, T., Haumann, F. A., Li, Q., Marshall, J., Muilwijk, M., Pauling, A. G., Purich, A., Smith, I. J., and

https://doi.org/10.5194/egusphere-2025-3666
Preprint. Discussion started: 16 September 2025

Thomas, M.: The Southern Ocean Freshwater release model experiments Initiative (SOFIA): Scientific objectives and experimental design, , https://doi.org/10.5194/egusphere-2023-198, 2023.

The IMBIE Team: Mass balance of the Antarctic Ice Sheet from 1992 to 2017, Nature, 558, 219–222, https://doi.org/10.1038/s41586-018-0179-y, 2018.

User Engagement and Services Branch: Extended Reconstructed Sea Surface Temperature (ERSST) Monthly Analysis, Version 3b, https://doi.org/10.7289/V5Z31WJ4, 2010.

Velicogna, I., Mohajerani, Y., A, G., Landerer, F., Mouginot, J., Noel, B., Rignot, E., Sutterley, T., van den Broeke, M., van Wessem, M., and Wiese, D.: Continuity of Ice Sheet Mass Loss in Greenland and Antarctica From the GRACE and GRACE Follow-On Missions, Geophysical Research Letters, 47, https://doi.org/10.1029/2020gl087291, 2020.

Vignon, É., Roussel, M. -L., Gorodetskaya, I. V., Genthon, C., and Berne, A.: Present and Future of Rainfall in Antarctica, Geophysical Research Letters, 48, https://doi.org/10.1029/2020gl092281, 2021.

Wang, D., Ma, H., Li, X., Hu, Y., Hu, Z., An, C., Ding, M., Li, C., Jiang, S., Li, Y., Lu, S., Sun, B., Zeng, G., van den Broeke, M., and Shi, G.: Sustained decrease in inland East Antarctic surface mass balance between 2005 and 2020, Nat. Geosci., 18, 462–470, https://doi.org/10.1038/s41561-025-01699-z, 2025.

Wang, W., Shen, Y., Chen, Q., Wang, F., and Yu, Y.: Spatiotemporal mass change rate analysis from 2002 to 2023 over the Antarctic Ice Sheet and four glacier basins in Wilkes-Queen Mary Land, Sci. China Earth Sci., 68, 1086–1099, https://doi.org/10.1007/s11430-024-1517-1, 2025.

Wang, Y. and Xiao, C.: An Increase in the Antarctic Surface Mass Balance during the Past Three Centuries, Dampening Global Sea Level Rise, Journal of Climate, 36, 8127–8138, https://doi.org/10.1175/jcli-d-22-0747.1, 2023.

Wille, J. D., Favier, V., Gorodetskaya, I. V., Agosta, C., Baiman, R., Barrett, J. E., Barthelemy, L., Boza, B., Bozkurt, D., Casado, M., Chyhareva, A., Clem, K. R., Codron, F., Datta, R. T., Durán-Alarcón, C., Francis, D., Hoffman, A. O., Kolbe, M., Krakovska, S., Linscott, G., Maclennan, M. L., Mattingly, K. S., Mu, Y., Pohl, B., Santos, C. L.-D., Shields, C. A., Toker, E., Winters, A. C., Yin, Z., Zou, X., Zhang, C., and Zhang, Z.: Atmospheric rivers in Antarctica, Nat Rev Earth Environ, 6, 178–192, https://doi.org/10.1038/s43017-024-00638-7, 2025.

Wills, R. C. J., Dong, Y., Proistosecu, C., Armour, K. C., and Battisti, D. S.: Systematic Climate Model Biases in the Large-Scale Patterns of Recent Sea-Surface Temperature and Sea-Level Pressure Change, Geophysical Research Letters, 49, https://doi.org/10.1029/2022gl100011, 2022.

https://doi.org/10.5194/egusphere-2025-3666
Preprint. Discussion started: 16 September 2025

Winkelmann, R., Levermann, A., Martin, M. A., and Frieler, K.: Increased future ice discharge from Antarctica owing to higher snowfall, Nature, 492, 239–242, https://doi.org/10.1038/nature11616, 2012.

Yeager, S. G., Chang, P., Danabasoglu, G., Rosenbloom, N., Zhang, Q., Castruccio, F. S., Gopal, A., Cameron Rencurrel, M., and Simpson, I. R.: Reduced Southern Ocean warming enhances global skill and signal-to-noise in an eddy-resolving decadal prediction system, npj Clim Atmos Sci, 6, https://doi.org/10.1038/s41612-023-00434-y, 2023.

Yin, Z: IceZYin/2023-AIS-SMB-CESM2: Initial release, Zenodo, https://doi.org/10.5281/ZENODO.16541813, 2025.

Yin, Z., Herrington, A. R., Datta, R. T., Subramanian, A. C., Lenaerts, J. T. M., and Gettelman, A.: Improved Understanding of Multicentury Greenland Ice Sheet Response to Strong Warming in the Coupled CESM2-CISM2 With Regional Grid Refinement, J Adv Model Earth Syst, 17, https://doi.org/10.1029/2024ms004310, 2025.

Zhang, X. and Deser, C.: Tropical and Antarctic sea ice impacts of observed Southern Ocean warming and cooling trends since 1949, npj Clim Atmos Sci, 7, https://doi.org/10.1038/s41612-024-00735-w, 2024.

Zhai, Z., Wang, Y., Lazzara, M. A., Keller, L. M., and Wu, Q.: Snow Accumulation Variability at the South Pole From 1983 to 2020, Associated With Central Tropical Pacific Forcing, JGR Atmospheres, 128, https://doi.org/10.1029/2023jd039388, 2023.

Zwally, H. J., Giovinetto, M. B., Beckley, M. A., and Saba, J. L.: Antarctic and Greenland drainage systems, GSFC Cryospheric Sciences Laboratory [data set], https://earth.gsfc.nasa.gov/cryo/data/polar-altimetry/antarctic-and-greenland-drainage-systems (last access: 1 August 2022), 2012